Palaeogeography, Palaeoclimatology, Palaeoecology 655 (2024) 112531

Contents lists available at ScienceDirect

Palaeogeography, Palaeoclimatology, Palaeoecology

journal homepage: www.elsevier.com/locate/palaeo

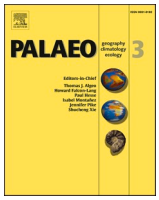

Holocene hydroclimate variability reconstructed from Lake Pangodi sediments in Estonia

Mariliis Eensalu [a,b,*], Nathan D. Stansell [a], Hannes Tõnisson [c], Jaanus Terasmaa [c], Egert Vandel [c], Tiit Vaasma [c], Eric S. Klein [d], Cameron R. Kuhle [d], Daniel B. Nelson [e]

[a] Department of Earth, Atmosphere and Environment, Northern Illinois University, USA
[b] Department of Geology, Tallinn University of Technology, Estonia
[c] Institute of Ecology, Tallinn University, Estonia
[d] Department of Geological Sciences, University of Alaska Anchorage, USA
[e] Department of Environmental Sciences, University of Basel, Switzerland

ARTICLE INFO

Editor: Paul Hesse

Keywords:
Baltic region
Europe
Lake level
Paleolimnology
Sedimentology
Quaternary

ABSTRACT

Long-term hydroclimate variability recorded in lake sediments from Estonia provide information about environmental changes in northern Europe during the Holocene. Lake Pangodi is a semi-closed basin lake in southern Estonia with a large surface area to volume ratio, making it sensitive to effective moisture balance (precipitation minus evapotranspiration), which is recorded as changes in the lake level. Here we conducted a ground penetrating radar (GPR) survey, sedimentological analyses, radiometric dating and lake level modeling study to identify periods of lake-level high- and low-stands. The radiocarbon-dated sedimentary stratigraphic features on our radargram support the model results, suggesting that Lake Pangodi formed at ~12.8 ka. The water levels were likely variable during the early Holocene, and the comparison of Lake Pangodi sediment facies and the lake level model show relatively stable lake water depth between ~9.8 ka and ~2.4 ka, and an increase towards modern. A notable reduction in lake levels occurred between ~8.2 and ~7.7 ka, likely due to a significantly reduced precipitation-evaporation balance. Our middle Holocene reconstruction suggests water column depths nearly 2.0 m lower than modern. This aligns with the results from studies conducted in the Baltic region, yet contrasts those from Scandinavia, suggesting different hydroclimate driving mechanisms during the Holocene variations in hydrogeological regimes. Our model detected the most abrupt rise of 1.7 m in water levels between ~1.5 and ~1.3 ka. This study highlights the need to develop proxies from single lake basins combining multiple methods for a better spatiotemporal resolution of paleo-hydrological changes.

1. Introduction

1.1. Climate change in Northern Europe

The impacts of recent climate change in high latitude regions are amplified compared to the lower latitudes (Shirley et al., 2022), leading to accelerated sea ice loss and permafrost thaw, which contributes to the increasing global temperatures. In response to the rapid modern warming, the northern European region is projected to experience a ~15 % increase in rainfall by the end of this century (Räisänen, 2016). However, such future climate projections often lack a longer-term perspective of the past drivers and responses of environmental changes, which could be studied using paleo-archives, such as lake sediments. Paleoclimate records are used for uncovering long-term information about the timing and magnitude of past hydrological changes, which will help predict climate variability under different boundary conditions. Ultimately, these records provide context for the range of potential hydroclimate variability that relates to modern versus natural climate warming.

1.2. Holocene climate in Northern Europe

The Baltic region became ice free by ~13.3 ka as the Scandinavian Ice Sheet retreated to the high latitudes of Europe (Raukas, 2009). The Holocene, that spans the last ~11.7 ka (thousands of calendar years before 1950 CE), is sub-divided here based on the classification of

* Corresponding author at: Department of Earth, Atmosphere and Environment, Northern Illinois University, USA.
E-mail address: meensalu@niu.edu (M. Eensalu).

https://doi.org/10.1016/j.palaeo.2024.112531
Received 5 March 2024; Received in revised form 11 September 2024; Accepted 30 September 2024
Available online 2 October 2024
0031-0182/Published by Elsevier B.V.

Walker et al. (2012) as the early Holocene (11.7 to 8.2 ka), middle Holocene (8.2 to 4.2 ka) and late Holocene (4.2 ka to modern). The early Holocene experienced a significant rise in temperatures in the Northern Hemisphere, which resulted in increasing ice melt in Scandinavia, the formation of kettle lakes in the northern Baltic region, and overall higher lake levels associated with wetter conditions (Björck et al., 1996). Following a brief ~200-year cold reversal period known as the Preboreal Oscillation at ~11.3 ka (Björck et al., 1996), northern Europe experienced a relatively warm phase during the Holocene thermal maximum (HTM) between ~11 and ~5 ka. Although there was summer insolation maxima in the Northern Hemisphere during that period, warming was delayed in the middle and high latitudes for 1 to 2 ka due to cooling from the remnant Laurentide Ice Sheet (Renssen et al., 2012).

Paleoclimate simulations and reconstructions agree that warm conditions prevailed in northern Europe from 8 to 6 ka (Heikkilä and Seppä, 2010; Poska et al., 2014), yet quantitative reconstructions of hydroclimate are still uncommon. Pollen-based reconstructions suggest the middle Holocene in the northern European region was relatively warm and dry as a result of decreased precipitation and/or increased evaporation (Seppä et al., 2009). Paleo-proxies from the Baltic region and neighboring areas show that some lake levels during the middle Holocene were generally lower (Digerfeldt, 1988; Punning et al., 2003, 2005; Sohar and Kalm, 2008; Terasmaa, 2011) yet others relatively higher (Saarse and Harrison, 1992; Saarse et al., 1995 and references therein). Thus, more records are needed to understand the relatively high degree of hydroclimate variability over the relatively short spatial scales during the middle Holocene because changes in water levels could also depend on local factors, such as catchment geomorphology and proximity to wetlands.

The late Holocene in northern Europe experienced a major change towards colder, wetter and more variable climate conditions due to declining summer insolation, changes in the atmospheric circulation patterns and increased moisture availability (Morley et al., 2014). Multiple studies have reported decreased lake levels and cold events between ~3.4 to ~3.2 ka in various locations in Estonia, as well as Sweden, and wetter conditions have been suggested between ~2.6 to ~1.9 ka, and after ~1.7 ka towards modern time (Saarse et al., 1995; Saarse and Rajamae, 1997; Hammarlund et al., 2003; Seppä and Poska, 2004; Punning et al., 2005; Sohar and Kalm, 2008; Street-Perrott et al., 2018).

1.3. Lake levels and moisture availability

Lake levels respond to shifts in the balance between local precipitation and evapotranspiration (known as moisture balance), and are often influenced by environmental parameters such as changes in the type of vegetation in the catchment area. This information about hydroclimate is often stored in lake sedimentary archives. This perspective is especially useful when studying past hydroclimate in a region where proxies from both semi-closed and open basin lakes are available. Large shallow (semi-)closed-basin lakes that have a large surface area to volume ratio are particularly sensitive to evaporation (Mason et al., 1994; Klein et al., 2005), while open basin lakes record precipitation with a minimal sensitivity to evaporation (Gat, 1996). Comparing sediment archives from both types of lake basins in the same region would therefore provide a more detailed view into the trends and magnitude of evaporative conditions in the past and moisture source variability.

1.4. Ground penetrating radar (GPR) and lake level reconstruction methods

Ground penetrating radar (GPR) is an efficient means for inferring lake level variations in the sedimentological record. This non-destructive method for acquiring high-resolution radargrams can provide direct evidence of sedimentary stratigraphy (Spencer et al., 1984) that can be used to identify shifting facies and ideal coring locations. For example, the configuration and continuity of the reflectors on the radargram show various lapout features, which can be radiocarbon (^{14}C)-dated and used as direct evidence of past shoreline or lake level elevation changes (Miall, 2010). The sediments can then be analyzed for organic matter, clay, silt and sand layers to determine their sedimentation during the studied time intervals by aligning the sedimentary stratigraphy with the reflector lines on the radargram (Digerfeldt, 1988; Magny et al., 2003). The ^{14}C-dates and sedimentary characteristics can then be combined into a single derivative by applying a lake level reconstruction model (Pribyl and Shuman, 2014).

1.5. Current study

Here we investigate the local hydroclimatic variability at Lake Pangodi in Estonia over the Holocene by reconstructing precipitation over evaporation (P-E) ratio and changes in the lake level. We used radar sounding and lake sediment analyses to identify local changes in past lake levels. We then employed a previously developed lake level model by Pribyl and Shuman (2014), and modified it to be used with both organic matter flux and total concentration data. We then compare our reconstruction to other paleo-records in the region. Our new record adds to the spatiotemporal coverage of paleo-hydrological variability in the Baltic region after deglaciation.

2. Study site

2.1. Location and lake morphology

Lake Pangodi (Fig. 1) is located in the northern part of Otepää Upland, south-eastern Estonia (58°11′46″ N, 26°34′12″ E). The semi-closed-basin lake sits on a topographic high at 106.3 m above sea level (EH2000 height system) with a surface area of about 935,000 m^2 (including 2 islands of 4000 m^2), and the lake has a water volume of approximately 3,697,000 m^3, maximum water depth of 10.0 m, and a mean depth of 3.97 m (Vaasma and Vandel, 2024). The watershed area of the lake is 7.6 km^2, and the estimated water residence time is ~1 year (Keskkonnaagentuur, 2022). Lake Pangodi is fed by a few small springs close to the shore. During higher water levels there is an outflow that forms in the SE sub-basin of the lake, called Hurda Bay (Fig. 1). Lake Pangodi formation took place after the retreat of the Scandinavian ice sheet, at ~14 ka (Kalm et al., 2011). The lake basin is a hummocky moraine complex of Quaternary deposits that is underlain with Devonian sandstone and Silurian limestone (Nestor et al., 1997). Lake Pangodi shores are steep and sandy with a few wetlands near the SW and E shores. Plants are found throughout the littoral zone except for a few sandy beaches that are in frequent public use.

2.2. Local climate

Estonia is located in a transitional zone between continental and maritime climate where changing westerlies have a profound effect on the environmental conditions. The local climate is mainly affected by the cyclonic activity originating from the northern Atlantic (Jaagus and Kull, 2011). One of the main controls on Estonian climate is the Gulf Stream, bringing milder weather to the Baltic region year-round, keeping winters warmer and summers cooler (Rossby, 1999; Jaagus, 2006). The North Atlantic Oscillation has a strong impact on European climate with the positive phase (higher than normal pressure difference between the Azores High and Icelandic Low) resulting in stronger westerly winds and relatively warmer and wetter conditions in the northern European region; the negative phase would indicate the opposite as the more meridional jet streams bring colder and drier conditions from the high northern latitudes of the Atlantic ocean (Lamb and Peppler, 1987). Other internal modes of variability affecting the region are the Arctic Oscillation, a dominant mode of atmospheric circulation that extends

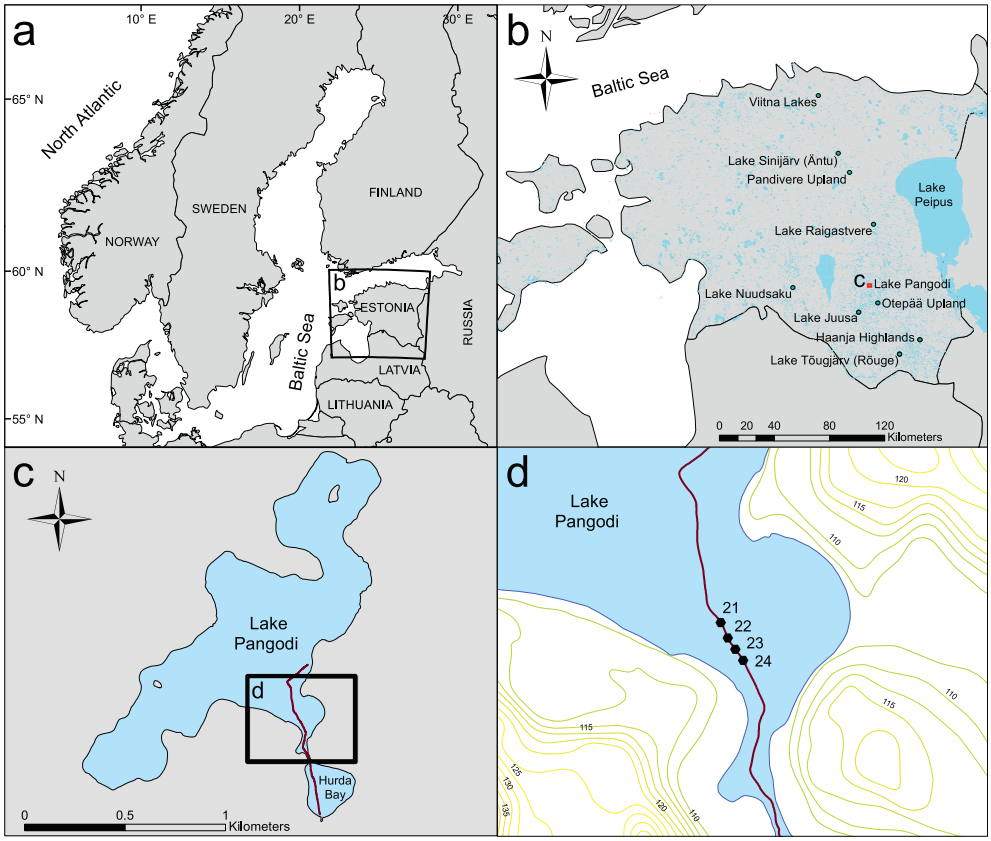

Fig. 1. Map of northern Europe (a) with Estonia marked as a square (b). Red small square on panel b marks the location of Lake Pangodi (c), and other records or center locations for highlands/uplands discussed in the text are highlighted as green filled circles. Panel c shows the GPR transect #20 as a purple line. Bottom right panel (d) is a blowout of panel c with ground elevation information (meters above sea level), and the same GPR transect, which is overlain by black filled hexagons that denote coring locations. (For interpretation of the references to color in this figure legend, the reader is referred to the web version of this article.)

over the extratropical Northern Hemisphere (Jaagus, 2003), and Scandinavia pattern, which is characterized by a large-scale seesaw-like pattern of atmospheric pressure differences between Scandinavia and Russia (Wibig, 1999). The Scandinavia pattern can significantly influence fluctuations in winter temperature and precipitation patterns across Northern Europe. During its positive phase, the Scandinavia pattern tends to bring colder air from the Arctic to Western Europe, resulting in colder winters and increased winter precipitation, while its negative phase is associated with warmer temperatures and reduced precipitation over the same region (Wibig, 1999).

According to the nearest meteorological station to Lake Pangodi (Tartu-Tõravere), the long-term (1991 to 2020) mean warm (May to October) and cold (November to April) season temperatures range between 13 °C and − 0.7 °C, respectively (EEA, 2024). Local precipitation amounts for the warm and cold periods total 262 mm and 411 mm, respectively. Total yearly precipitation in Estonia varies at ~660 mm per year, which is similar to the precipitation amounts at Pangodi. Precipitation exceeds the annual evaporation by ~25 % (http://www.ilmateenistus.ee/kliima/). The instrumental climate data from Estonia show warming and increased precipitation trends since 1951 as the westerlies have been intensifying during the cold seasons (October to April), and decreasing in May (Jaagus et al., 2017). Since 1951, a decrease in northerly circulation has been observed during March and October, and these climate trends have led to warmer winters which occur in hand with increased precipitation (Jaagus et al., 2017). On longer (centennial to millennial) time-scales, northern European climate has likely been affected by changes in the solar insolation, the Atlantic Meridional Overturning Current (AMOC) heat transport (Marshall et al., 2001; Paul and Schulz, 2002), internal modes of variability, and the consequent prevailing winds and precipitation patterns (Jaagus, 2003).

3. Methods

3.1. Ground penetrating radar

Geophysical profiling at Lake Pangodi was carried out from a boat using a high-resolution CrossOver CO730 GPR manufactured by ImpulseRadar, with antennae operating at dual-band 70/300 MHz frequencies. Data from the antennae were monitored and recorded using the ImpulseRadar ViewPoint application on a Samsung Galaxy Tab Active 2 that was wirelessly connected to the GPR. The GPR traces (radargrams) were continuously recorded every 2 s, along with a paired location marker from an onboard GPS unit (accuracy mostly between 0.2 and 0.5 m). Recorded penetration depth for the 70 MHz frequency was 12 m. The radargram recorded at 300 MHz was deemed not helpful and was therefore excluded from this study. The GPR signal naturally attenuated with increasing water and sediment depth but variations in dielectric properties between subsurface facies enabled their distinguishment. A total of 27 profiles were recorded and visually enhanced in R using a package RGPR (Huber and Hans, 2018). Direct measurements of sediment surface depths (described below) were used to calibrate the radar velocity which resulted in an average sub-surface velocity of 0.035 m ns^{-1}, falling within the range of previously reported results in lake sediment and peat studies (Parry et al., 2014; Corradini et al., 2020).

3.2. Radargram analysis

The GPR subsurface imaging helped identify suitable coring locations with sediment deposits that record lake level variations through time. The Hilbert transform function was applied to all profiles to

identify possible sandy versus silty layers in the sediments as it enhances the visual contrast between different layers. The profiles were then visually analyzed for sections with multiple lapouts and unconformities in a near shore environment. For example, sequences below a discontinuity such as toplaps were characterized as a termination against an overlaying strata, and interpreted as areas of possible erosion or lack of deposition; truncation indicating post-depositional erosion or strata deposition with subsequent tilting and erosion was identified where GPR reflectors terminated along an unconformity surface (Mitchum, 1977). Above discontinuity sequence boundaries, onlaps were identified as reflection patterns showing shallow dipping strata against more steeply dipping older layers, while downlaps indicate initially inclined strata terminating downdip. Offlaps were characterized as reflection patterns of strata which prograde to deeper depths and terminate in the deep basin (Mitchum, 1977; Christie-Blick, 1991). Radargram from transect #20 (Fig. 1) was perpendicular to the shoreline and had multiple areas with various visible lapouts. This transect showed the most pronounced evidence of lake level changes, and was therefore selected for further investigation by sediment core collection.

3.3. Sediment core collection

Lake Pangodi sediment cores were collected from a boat along a GPR transect #20 to analyze the shore deposits visible on the radargram. Each coring location was selected at an interval of ~15 to ~20 m apart. Secchi and sediment surface depth were recorded at each coring location. Surface sediments were not collected. A total of 4 lake sediment cores labeled 21, 22, 23 and 24 were collected 32, 22, 22 and 47 cm below the surface of the sediment-water interface, which was 350, 337, 302 and 262 cm below the lake water surface for each of the cores, respectively. The composite depths of cores 21, 22, 23 and 24 were 419, 387, 238 and 172 cm, respectively. Coring at each location was undertaken with a 1-m-long modified square-rod piston corer until the basal sand and clasts prevented retrieving additional core sections. Sediment was cored within a ~50 cm radius to retrieve sections with a 20 cm overlap.

3.4. Laboratory analyses

The collected sediment cores were split vertically in the lab, and the color defined based on Munsell soil color charts (Kipfer, 2021). The cores were then photographed on a smartcube® Camera Image Scanner SmartCIS equipped with a 50 mm lens to obtain high-resolution (300 dpi) color image scans (RGB), which were then visually enhanced in Adobe Illustrator CC. Each core was visually inspected for grain size and color at 0.5 cm intervals.

Sedimentological analysis was performed on all core sections, and all analyses were carried out at the same sample intervals. Dry bulk density (g cm^{-3}) was measured from 1 cm^3 sediment samples ($n = 528$) at 3 cm intervals in two of the deeper cores (21 and 22) and at 2 cm intervals in the shallower cores (23 and 24). XRF analysis was carried out on the same 1 cm^3 dry sediment samples using a handheld XRF Olympus Innov-X instrument. Magnetic Susceptibility (MS) measurements were conducted on dried sediment samples from all core sections using an ASC core analysis system running on MAGTRAK software. LOI analysis was done on the previously dried sediments using a muffle furnace (Dean Jr, 1974). The samples were heated to 550 °C for four hours and weighed to determine the amount of organic matter (OM). Net sedimentation rates were calculated by dividing the difference between two consecutive depth values with the corresponding calibrated ages. The OM flux (g y^{-1} cm^{-2}) was calculated by multiplying the weight percent LOI (550 °C) value by bulk density (g cm^{-3}) and sedimentation rate (cm y^{-1}). The heating process was repeated at 1000 °C for two hours to determine the amount of liberated CO_2. From this, calcium carbonate content could be calculated by multiplying the weight loss by 2.274, i.e., the molecular weight ratio between $CaCO_3$ and CO_2 (Loeppert and Suarez, 1996). The remaining sediment fraction (after 1000 °C) is referred to as residuals.

We used field notes, sediment images, loss-on-ignition (LOI) and x-ray fluorescence (XRF) data to identify stratigraphic overlap for each section among the four cores. The split sediment cores were lined up in the laboratory based on field notes, and each overlap was checked visually. The LOI and XRF data from each core section were inspected for any discrepancies prior any data analyses as a secondary verification measure for determining the overlapping stratigraphy.

3.5. Lake Pangodi chronology

A total of 14 radiocarbon (^{14}C) samples of plant macrofossil remains from the four cores were analyzed to establish a chronology of lake level changes. The ^{14}C samples underwent a standard acid-base-acid treatment (Abbott and Stafford, 1996) prior to combustion at Northern Illinois University. The samples were then converted to graphite and measured at the W.M. Keck Carbon Cycle AMS Laboratory at the University of California, Irvine. An age-depth model was developed for each of the four lake sediment cores using BACON software (Blaauw and Christen, 2018) and IntCAL20 dataset (Reimer et al., 2020) in R Studio. We report the minimum and maximum ages on the age-depth scale with 95 % confidence intervals, and we refer to the mean BACON-modeled ages throughout the text. The calibrated modeled ages presented as thousands of years before present (ka) are relative to 1950 CE.

3.6. Data analyses

We performed principal component analysis (PCA) on the sedimentological and bulk geochemical data (14 variables with >88 data points in each core) using R package FactoMineR (Lê et al., 2008). Data standardization was done automatically by the R package prior to running the covariance PCA on the LOI, MS and XRF (Si, K, Ca, Ti, Mn, Fe, Rb, Sr, Zr and light elements – LE) data. We also used sequential regime shift detection software (v. 6.2) with a 95 % confidence level and Huber's tuning constant of 1 to detect statistically significant shifts in all time-series (Rodionov, 2004). We report weighted mean values of the regime shift analysis with data cutoff lengths of 20 for XRF and OM flux, 30 for OM, and 40 for lake level reconstruction and P-E balance. Insolation was modeled using Acycle package in Matlab (Li et al., 2019).

3.7. Lake level model

Past lake level heights at Lake Pangodi were reconstructed using the GPR profiles and sediment composition. We constrain the lake level heights (elevation relative to modern) by identifying littoral, transitional and deep water sediments within the four cores from transect #20, following the model outlined by Marsicek et al. (2013). Our reconstruction is based on the rationale that coarser grains (sand) accumulate near the shores, and finer (silt and clay) in the deep-water environment. The waves carry enough energy to accumulate sandy material in the shores due to the upward-moving water while carrying smaller particles such as silt and OM to the deeper parts of the basin by downward-moving water (King and Williams, 1949).

Previous studies (Marsicek et al., 2013; Pribyl and Shuman, 2014; Parish et al., 2022) have used OM content to model the lake level where littoral, transitional and deep-water facies were defined as up to 35 %, 35 to 75 % and over 75 % OM, respectively. Based on LOI analyses, the OM content in our data set range between 0.2 and 87 %. However, we use OM flux (ranging between 0 and 0.35 g y^{-1} cm^{-2}) as the input variable to model Lake Pangodi water level throughout the Holocene (see Section 4.3. for details). Here we assign OM flux values ranging from 0 to 0.12 g y^{-1} cm^{-2} (low) for littoral sediment, 0.12 to 0.23 g y^{-1} cm^{-2} (medium) for transitional sediments, and 0.23 to 0.35 g y^{-1} cm^{-2} (high) for deep-water sediments.

Previous studies have used a 5 % step (iteration $n \leq 6$) for providing uncertainty estimates to the past lake level change using OM content

(Newby et al., 2011; Marsicek et al., 2013; Pribyl and Shuman, 2014; Parish et al., 2022). We adjusted the upper limits of OM flux for Lake Pangodi littoral to transitional facies shifts ±20 % between each iteration (10 % step, $n = 5$) and by ±10 % between each iteration for the transitional to deep-water facies shifts (5 % step, n = 5). We increased the littoral to transitional facies uncertainty estimate from 5 % to 10 % because the OM flux has not been used as an input variable in a lake level model before (Fig. 2). Increasing the transitional to deep-water facies boundary limit did not notably change the model output, therefore it was kept at 5 %.

Lake Pangodi water level change was constrained by averaging the 50-year OM flux values from all cores meeting the model criteria. As the model results demonstrated the highest and stable water levels (elevation) between ~1.3 and ~0.7 ka (169 ± 6 cm below modern lake surface, hereafter bmls), we make the assumption that it is representative of the modern lake level, and therefore shifted the model output by 169 cm to higher values, so that the modern lake level value equals 0 ± 6 cm instead of 169 ± 6 cm. We apply this approach because there were no sediments retrieved from the topmost sediments in our cores. Water column depth (CD) at our sampling locations was calculated by subtracting the sediment elevation from the modeled lake level at 50-year time steps.

For comparison, we also modeled the lake level using OM only (after Pribyl and Shuman, 2014), not flux. The littoral, transitional and deep-water facies were defined as up to 35 %, 35 to 75 % and over 75 % OM, respectively. In this case, the upper limit OM values for Lake Pangodi littoral to transitional facies shifts were changed by 5 % between each iteration (n = 5) and by 5 % between each iteration for the transitional to deep-water facies shifts (n = 5), and the lake water residence time was set to 0.5 to 1.5 years.

3.8. Moisture balance reconstruction

The past lake levels were assumed to be equal to water column depth changes (difference between the lake surface elevation and the sediment-water interface; Δ_{Depth}) which was used as an input variable to model lake water mass balance throughout the Holocene. The reconstructed sediment-surface interface was calculated based on core 21 data, for which the modern sediment-surface interface lies at 350 cm bmls.

Since the separate effects of precipitation (P) and evapotranspiration (E) in the Lake Pangodi basin could not be constrained, we calculate the balance between the two as one variable, P-E balance. The sand and silt boundaries were defined first as indicators of low and high lake water column depths (Δ_{Depth}) in each core, respectively, with the assumption that the coarse grain sand boundary reflects shallow waters (< 1 m) throughout the existence of the lake. The lake volume change (ΔV) is a function of the Δ_{Depth} multiplied by the lake surface area (S). The ΔV is defined as follows:

$$\Delta V = \Delta_{Depth} \times S = \Delta P - E \times A_B \times \Delta T \quad (1)$$

where the P-E balance (ΔP-E) is a combined variable that represents the net effect of both precipitation and evapotranspiration (mm y^{-1}), A_B is the area of lake basin in m^2 and ΔT is the lake water residence time in months. Although Lake Pangodi basin has an irregular shoreline, the lake shores are steep, and therefore we chose to use the equation above, which treats the basin morphometry as a cylinder-shaped object.

4. Results

4.1. Radar-derived stratigraphy and lapout features

The radargrams of Lake Pangodi sediments aided in selecting sediment coring locations and identifying sedimentary features. The collected scan reveals stratified sediments across the entire transect #20 profile in the main lake basin (Fig. 3). The radar penetrated stratified lake sediments, but there was a lack of a return signal for the deeper strata (> 7 m). The lowest reflectors in the lower part of the cores correspond to sand layers identified in the core samples. A well-defined continuous reflector line appears to connect the topmost sediment layers in cores 21, 22 and 23. Although highest in elevation, the core 24 sediments were acquired from just below these continuous features (Fig. 3). In core 24, there are onlaps between ~340 cm and ~380 cm bmls. Below these, several truncation-like features can be seen, and some of the younger layers in core 24 have possibly been eroded. The same onlap surface can be observed cores 23 and 22 (Fig. 3). Near core 23, there is a toplap at ~340 cm and offlaps between ~460 and ~490 cm bmls. In core 22, there are three offlaps identified between ~510 cm and ~540 cm bmls. On top of the middle offlap, one onlap was identified at ~450 cm bmls in the same core. There are toplap features in core 22 above ~420 cm bmls, which can also be seen in core 21 (Fig. 3). The reflector geometries in core 21 suggest off- and downlap features in the bottom of the core below at ~730 cm bmls, and toplap/truncation above these until ~640 cm bmls. On top of that, several offlaps and toplaps were identified until ~580 cm bmls, and an onlap at ~540 cm bmls, the last of which can be seen across all cores (Fig. 3).

4.2. Radiocarbon results and core lithology

Fourteen radiocarbon dates were acquired from plant macrofossils from the four cores (Table 1, Fig. 4), resulting in mean modeled ages spanning the last ~12.8 ka. There were no macrofossils suitable for radiocarbon dating found in the lower sections of cores 22 and 24. According to the GPR reflector lines discussed above, the radiocarbon age of 7.8 ka in core 24 may be reworked from older sediments as the radargram suggests that this sample is from a core section with notable truncation features. The rest of the modeled radiocarbon dates are in a general agreement with the radargram. In addition to the possible disposition of the radiocarbon samples through reworking, the minor inconsistencies on the radargram (Fig. 3) may arise from a slight disposition of the coring location in respect to where the transect was recorded, or the vertical imprecision of the profile as the GPR signal velocity varies in different substances. For example, the average velocity interval for gyttja (0.045 ± 0.005 m ns^{-1}) is different from that of clays (0.037 ± 0.003 m ns^{-1}), as reported by Corradini et al. (2020). Therefore, slight differences between the core images and the radargram are expected.

Lake Pangodi sediments mainly consist of gyttja, sand, silt and clay (Fig. 5). The bottom of every core had sandy profiles for which the modeled ages were older than ~12.5 ka. In core 21, sands dominate in the bottom of the core at ~800 cm bmls (~13.0 ka), silt and clay layers mixed with sandy units appear above 750 cm bmls (after ~11.6 ka), and sediments above 690 cm bmls (~9.7 ka) are mostly gyttja. We also note two distinct charcoal layers at 796 and 781 cm bmls (~12.8 and ~12.4 ka). From ~9.7 ka (690 cm bmls) towards modern, the core 21 sediment record mostly consists of gyttja. Core 22 shows sand and silt below 640 cm bmls (~7.0 ka), and gyttja-rich layers above with some sandy gyttja appearing between 510 cm (~4.3 ka) and 460 cm bmls (~3.3 ka). Core 23 displays sand and clay units until 500 cm bmls (~7.8 ka), gyttja layers with varying sand content until 400 cm bmls depth (~7.8 to ~2.4 ka), and gyttja above. Core 24 features mostly clays and sands until 380 cm bmls (~7.3 ka), and organic rich gyttja layers above it (until ~1.0 ka).

The sediment facies were identified as shown in Table 2. For example, sections with gyttja did not have any visible lamination, were high in organic matter (OM) and had high OM flux values with low to medium magnetic susceptibility (MS) values (Figs. 5 and 6). Sandy gyttja was most abundant in core 23, and had medium to high OM content, yet low MS values. Silt and clay layers were observed in the bottom sections of each core, were low in OM, had generally increased MS values and showed faint and sporadic lamination. Sand particles

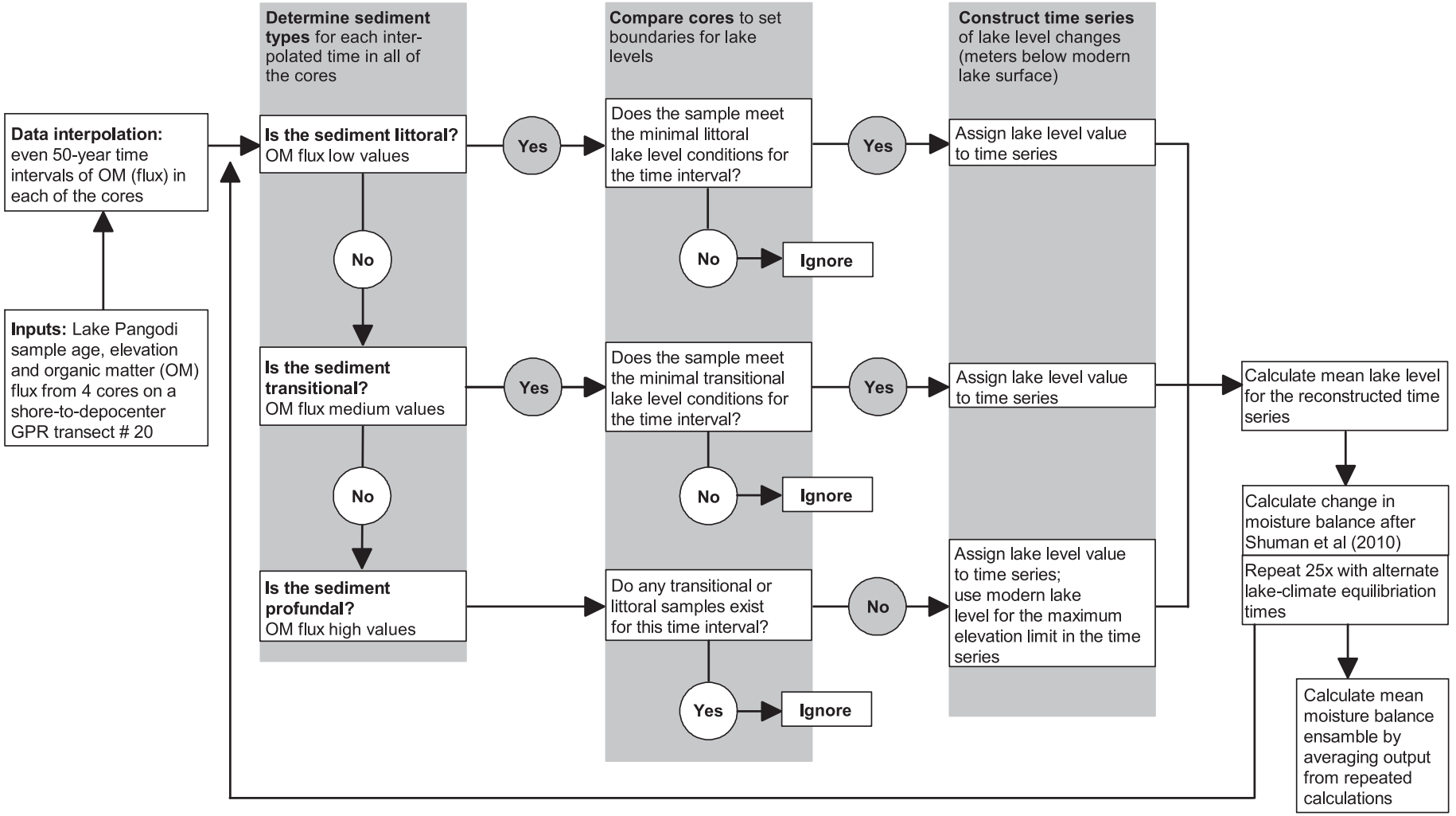

Fig. 2. Flow chart describing the utilization of Lake Pangodi organic matter (OM) flux (and OM data) from four sediment cores to create quantitative lake level and moisture budget reconstruction. Method and figure modified from Pribyl and Shuman (2014).

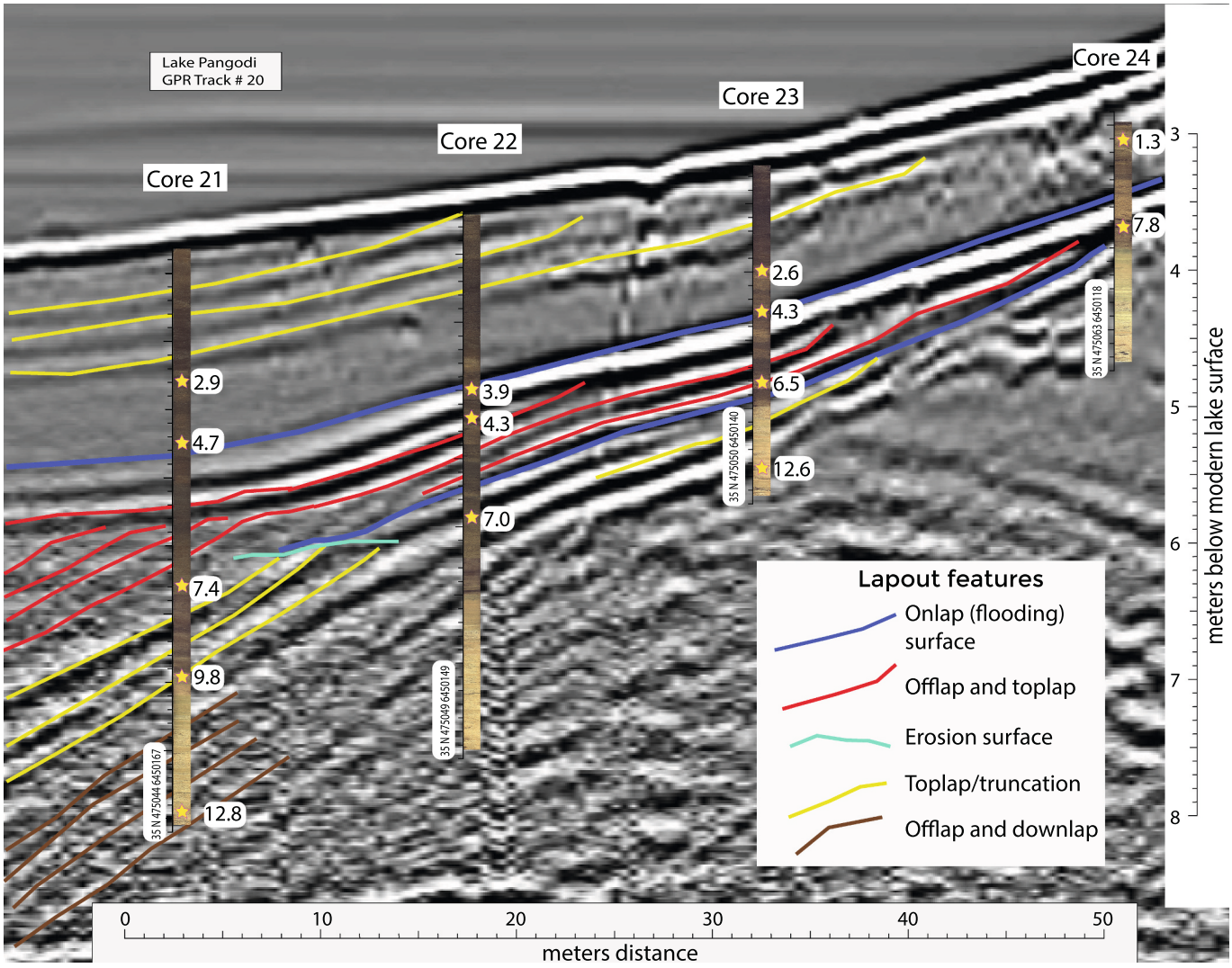

Fig. 3. Lake Pangodi radargram #20 section with sediment core locations 21, 22, 23 and 24 indicated by the sediment image overlays, the locations of which are also shown on Fig. 1. The x-axis shows distance along the transect starting from the north, y-axis on the right is the sediment depth below modern lake surface. The coring locations are in an area of multiple lapout features, defined after Boggs Jr. (2015), shown on the lapout features legend. Core GPS locations are written vertically at the bottom of the core images. Radiocarbon ages marked by yellow stars show *modeled* mean ages (ka BP). (For interpretation of the references to color in this figure legend, the reader is referred to the web version of this article.)

Table 1
Lake Pangodi radiocarbon ages from cores 21, 22, 23 and 24. Sample depth (cm) in the core is relative to the sediment-water interface and the depth below modern lake surface is abbreviated as bmls. Radiocarbon ages were calibrated using IntCal20 (Reimer et al., 2020), using the R package BACON (Blaauw and Christen, 2018). Minimum and maximum calibrated and modeled ages (years before 1950 CE) represent the 95 % range.

Core #	UCI Lab #	Material	Core depth (cm)	Depth mbls (cm)	Measured ^{14}C age	Measured error (±)	Min, median and max calibrated age	BACON modeled ages			
								median	min	mean	max
21	273,626	Seed/berry	128	478	2805	15	2773–2894-3015	2911	2806	2919	3116
21	273,627	Wood	174	524	4225	25	4557–4722-4887	4738	4528	4738	4912
21	269,626	Woody Debris	279	629	6480	20	7259–7376-7493	7370	7260	7376	7531
21	269,627	Woody Debris	346	696	8760	70	9484–9865-10,245	9771	9520	9792	10,159
21	269,628	Wood	445	795	10,920	25	11,602–12,657-13,711	12,815	12,745	12,829	13,041
22	273,628	Terrestrial plant fragment	149	486	3635	15	3821–3963-4104	3946	3832	3950	4079
22	273,629	Wood	170	507	3860	15	4132–4282-4432	4286	4159	4293	4408
22	269,629	Woody Debris	243	580	6140	20	6871–7027-7183	7025	6865	7036	7162
23	269,631	Seed shell	98	400	2450	20	2328–2537-2745	2563	2366	2550	2704
23	273,630	Seed/berry	128	430	3885	15	4124–4291-4441	4321	4158	4314	4409
23	269,632	Woody Debris	180	482	5725	45	6278–6522-6766	6524	6316	6531	6793
23	269,633	Grass fibers	243	545	10,650	25	12,480–12,633-12,785	12,675	12,203	12,631	12,732
24	273,631	Terrestrial plant fibers	60	322	1260	140	616–1164-1711	1252	912	1299	2029
24	269,634	Seed	124	386	7020	20	7682–7832-7981	7846	7694	7840	7929

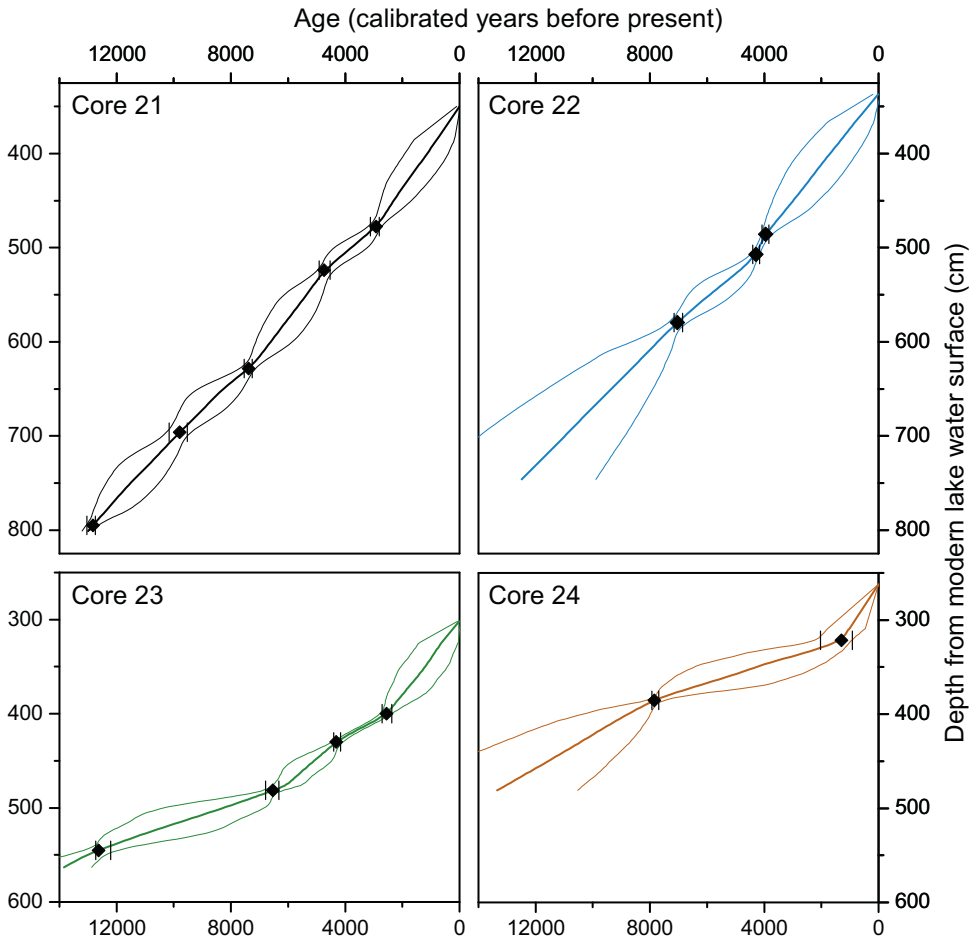

Fig. 4. Modeled age-depth scales of Lake Pangodi cores 21, 22, 23 and 24. The outer bounding lines represent 95 % confidence intervals and the middle line shows the mean modeled ages. Black filled symbols with error bars represent radiocarbon samples and the associated modeled min and max values.

ranged from small to coarse grained, and the MS values in these core sections were medium to high.

4.3. Organic matter, flux and magnetic susceptibility

The organic matter and OM flux data from Lake Pangodi cores is provided in Fig. 6, which also shows the MS profiles along with the composite core image scans. LOI measurements exhibit an increasing trend in OM values towards the modern, and high values of >50 % in the late Holocene. All four cores have low OM content (< 25 % LOI @ 550 °C) from the beginning of the record until ~6.6 ka. We report three regime shifts in core 21 OM content mean values increasing stepwise from 2 % before ~9.6 ka to 59 % after ~2.9 ka. Similar increases to higher average values were also detected in rest of the cores.

Based on the regime shift detection (not shown on figures), the average OM flux rates in core 21 increased from low to medium values at ~9.7 ka, and to high values at ~7.2 ka. The average values then decreased to medium at ~4.8 ka, and returned to high values after ~2.9 ka. In core 22, low average values were recorded until ~4.5 ka, and medium values thereafter towards modern time. In core 23 OM flux data, a shift from low to medium values was detected at ~2.4 ka, and a shift to high values at ~1.5 ka. The average OM flux values in core 24 were low across the entire record. When comparing the regime shift analyses applied to the OM and OM flux data across the entire core (original data on Fig. 6), these shifts do not align.

Magnetic susceptibility (MS) and sediment color description were used to describe Lake Pangodi sediments. The MS data measured on all four cores is shown on Fig. 6. The MS values were generally higher in the lower core sections that were older than ~9.5 ka, decreasing towards the surface. The color of Lake Pangodi sediments varied between 2.5Y 2.5/1 (black) and 10YR 5/2 (grayish brown). Lighter colors occurred in concert with higher MS values, except for core 23 where the average MS values in the dark-colored sediments increased at ~1.9 ka (Fig. 6).

4.4. Composite proxy record principal component analysis

The PCA performed on the individual cores illustrates that the difference in Lake Pangodi sediment geochemical properties increases with an increasing core sediment-water interface depth (Fig. 7 and Supplemental Figs. 2–4). When comparing Fig. 7 and Supplemental Figs. 2–4, the dual PCA axis 1 vs 2 plot demonstrated the most overlap between the early and late Holocene sections marked by pale blue and yellow ovals in core 21, and the least in core 24. The standardized Lake Pangodi PCA axis 1 scores are best correlated with Rb, Sr, Zr and K while PCA axis 2 scores correlate most with Fe in cores 21 and 22, and with Ca in cores 23 and 24 (Supplementary Table 1). The PCA axis 1 of deeper cores 21 and 22 are negatively well correlated with elements that have a low atomic number on the periodic table (LE), which is associated with OM content (Fig. 6). High correlation of K and Ca in cores 23 and 24 suggests that input of allogenic material from the landscape (erosion) has a greater impact on these archives. This is expected as cores 23 and 24 are shallower and located more towards the lake shore, therefore the allogenic material reaching the lake would be preferentially deposited there (Kylander et al., 2011). Additional correlation analysis results can be found in the supplementary materials.

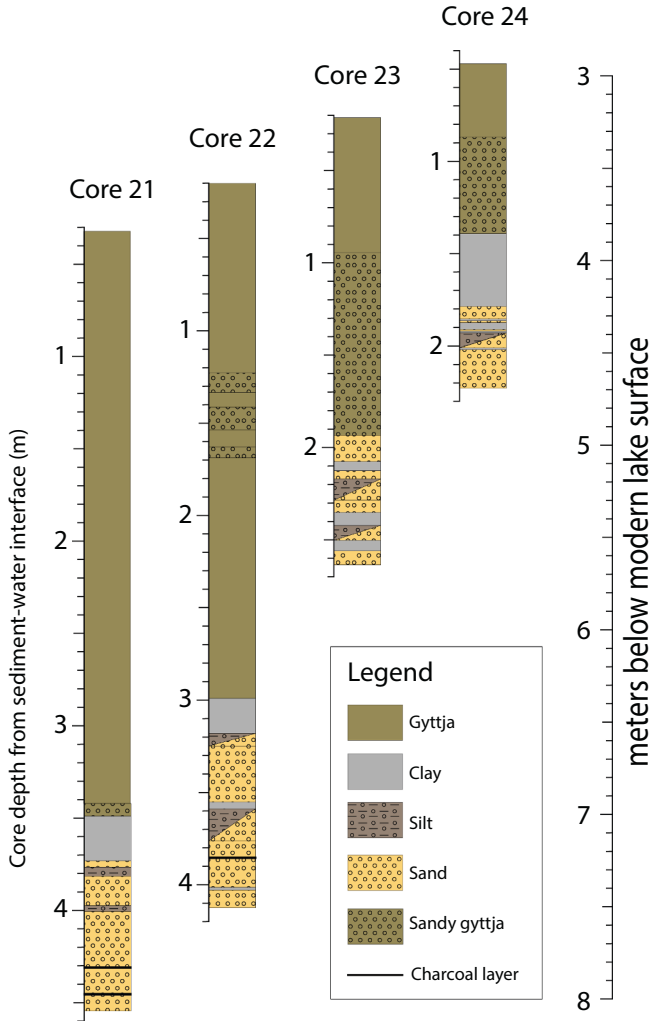

Fig. 5. Lake Pangodi sediment lithology in cores 21, 22, 23 and 24. Depth (m) from the sediment-water interface is shown on the left of each core.

4.5. Modeled lake level and water column depth

The OM flux model results indicate varying lake levels throughout the Holocene (Fig. 8 panel b). We highlight a period at ~8.2 ka when the lake Pangodi water level had reached the early Holocene maximum elevation of 415 ± 60 cm bmls (water column depth, or CD 230 cm), whereafter a decrease to 505 ± 70 cm bmls (CD 135 cm) occurred until ~7.7 ka. According to the reconstruction, the average lake level elevation was 375 ± 40 cm bmls during the middle Holocene, and 205 ± 70 cm bmls during the late Holocene. The average water CDs during the early (9.8 ka to 8.2 ka), middle (8.2 ka to 4.2 ka) and late (4.2 ka to modern) Holocene were 188, 206 and 247 cm, respectively. There is an ~70 cm decrease in the modeled lake level values from ~2.6 to ~2.5 ka, followed by a notable 140 cm (130 cm CD) increase from ~2.4 until ~2.2 ka. The model also suggested a sharp increase in water levels after ~1.4 ka as the OM flux displayed only sub-littoral and deep-water conditions thereafter. The regime shift detected five changes in the modeled lake level at ~7.4 ka, ~6.0 ka, ~4.5 ka, ~2.4 ka and ~1.5 ka with the mean lake level increasing from 475 to 390 to 335 to 300 to 185 to 20 cm bmls, respectively. The regime shift applied on the water CD values resulted in four shifts at ~7.4 ka, ~5.1 ka, 2.4 ka and ~1.5 ka, with the mean values increasing from 286 to 218, then decreasing to 191, and then increasing to 248, and to 375 cm, respectively. The most pronounced rise of 165 cm in the mean lake level (130 cm CD) occurred at ~1.4 ka. When we applied the regime shift with a minimal cutoff length (5), the model highlighted short periods of lower lake levels in comparison to the preceding periods between ~8.0 and ~7.6 ka, ~3.5 and ~3.1 ka, and ~2.6 and ~2.4 ka.

4.6. Lake Pangodi moisture balance (P-E) reconstruction

The water column depth results were used as an input variable to model the P-E balance of the Lake Pangodi watershed. Similar to the lake level model, the P-E reconstruction also displayed an increasing P-E trend throughout the Holocene. In comparison to the ~0.7 ka values, the average early (~9.8 to ~8.2 ka), middle and late Holocene P-E values were ~ −232, ~ − 207 and ~ −157 mm y^{-1}, respectively (Fig. 8 panel a). There were four regime shifts detected in the P-E balance data set at ~7.4 ka, ~5.1 ka, ~2.4 ka and ~1.5 ka, from ~ − 232 to ~ − 192 to ~ − 226 to ~ − 155 to ~ − 7 mm y^{-1} at ~5.9 ka, and to ~ − 13 mm y^{-1}, respectively. The reconstruction suggests that the P-E increased by ~320 mm over the entire Holocene.

5. Discussion

5.1. Water level changes inferred from sediment

The sedimentary characteristics of the four cores taken from Lake Pangodi provide detailed evidence of Holocene-spanning water level dynamics. The modeled basal ages of the deepest sediments in Lake Pangodi cores 21 to 24 indicate that the lake was established by ~12.8 ka. Sand in the bottom of these cores was most likely washed in from a nearby kame before lake stabilization, which probably took place at ~9.8 ka. We suggest this because the topmost sandy layer in core 21 featured a ^{14}C age of 9.9 ka, and sediment with increased OM content right above that layer indicates a stabilized vegetation presence in the lake basin. The sedimentary characteristics in cores 21 and 22 indicate that higher lake levels in these locations may have persisted between ~12.5 ka until ~9.6 ka, and lower water CD anywhere between from ~4.0 and ~3.3 ka. Sediments in cores 23 and 24 suggest a similar pattern with lower CD in these locations between 7.5 and ~4.3 ka, indicating no major increases in the water level during that time period. As the OM content increases towards the top of each core, these sections most probably reflect increased lake levels during the late Holocene.

Table 2
Sediment facies and a column with lake level interpretation.

Lithology	Organic matter content	Organic matter flux values	Magnetic Susceptibility	Depositional process	Interpretation
Gyttja (mud) with no visible lamination	High	High	Low to medium	Suspension	High lake level
Sandy gyttja (mud) with faint partial lamination	Medium to high	Medium to high	Low	Suspension and low wave deposition	Medium to high lake level
Sand, fine to coarse grained, no lamination	Low	Low to medium	Medium to high	Wave deposition	Low lake level (or sand redeposition from a nearby kame)
Silt, partial lamination	Low	Low	High	Suspension	High lake level
Clay	Low	Low	Medium to high	Slow suspension	Very high lake level

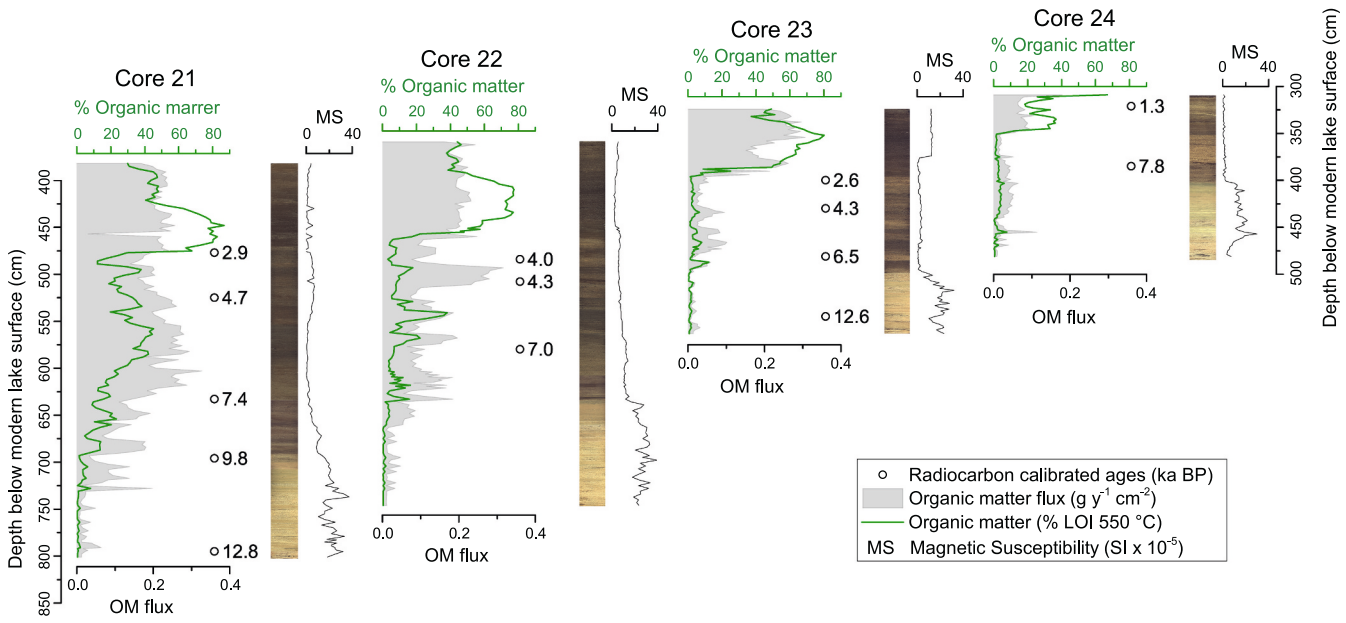

Fig. 6. Organic matter and magnetic susceptibility (MS) data along with core image scans and age data from Lake Pangodi cores 21, 22, 23 and 24. Organic matter (OM) flux is shown as gray shading. Open circles show the modeled radiocarbon ages before present (ka). See Supplemental Fig. 1 for organic matter, OM Flux and MS data plotted against age scales.

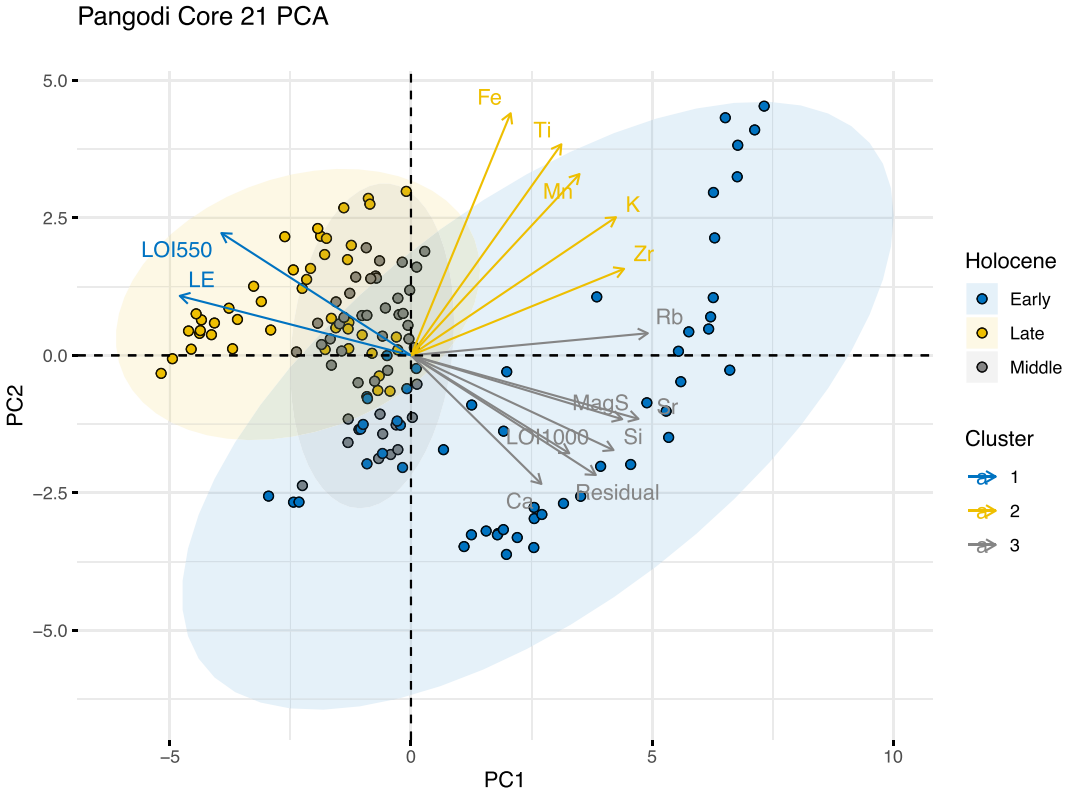

Fig. 7. Principal component analysis (PCA) of Lake Pangodi sediment core 21. Three sample clusters are defined on the biplot (principal component axes 1 vs 2) as the early, middle and late Holocene with the selected variables indicated by arrows, shown in three groups. PCA analyses of cores 22, 23 and 24 can be found in the supplemental material (Supplemental Figs. 2–4). In addition to elemental composition (Fe, Ti, Mn, K, Zr, Rb, Sr, Si and Ca), the PCA included Loss-on-Ignition (LOI) data at 550 °C and 1000 °C, the LOI residuals, light elements (LE) and magnetic susceptibility (abbreviated here as MagS).

When comparing core 23 to the rest of the cores, the lack of a distinct clay layer likely suggests that the presence of springs may have disturbed the sedimentation process. Furthermore, the PCA cluster overlap of the deeper cores 21 and 22 in comparison to cores 23 and 24 suggests that the sediments from the shore were likely transported to deeper areas, leading to mixing with the sediments in the deeper basin.

We speculate that in comparison today, the water level may have been higher during a short period over the last 1.5 ka as the LiDAR DEM

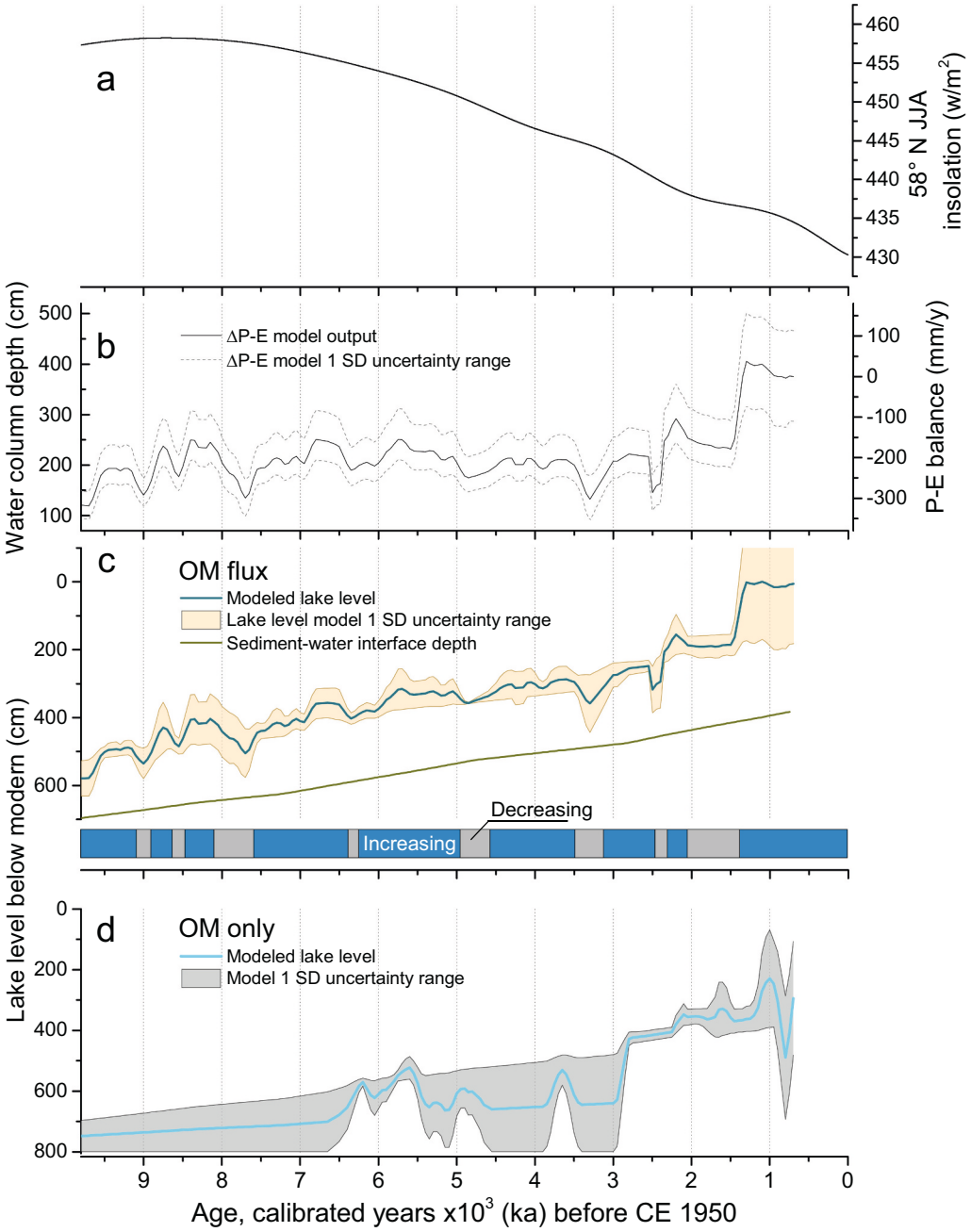

Fig. 8. Top panel (a) shows warm season (JJA) insolation at 58°N, modeled using R package Acycle. Second panel (b) represents the reconstructed change in precipitation over evaporation (P-E) balance (right axis), which was modeled based on the water depth calculated by subtracting the sediment-water interface depth values (left axis) from OM flux based modeled lake level values. The gray dashed lines signify 68 % uncertainty range. Third panel (c) shows reconstructed Lake Pangodi water level from organic matter (OM) flux as dark blue line. Range of uncertainty from 25 facies threshold simulations is shown as light orange. Sediment-water interface is shown as a green line. The horizontal gray-blue bar below panel c is an interpretation of the OM flux-derived lake level model where low and decreasing (gray) versus high and increasing (blue) lake levels represent at least a 15 cm shift in the mean modeled lake level. Bottom panel (d) shows the reconstruction (after Pribyl and Shuman, 2014) from OM only (not flux) as a light blue line and the gray area marks the model uncertainty range of 25 simulations. (For interpretation of the references to color in this figure legend, the reader is referred to the web version of this article.)

map (geoportal.maaamet.ee/eng/) of the lake shows a distinct terrasse feature on the shores. The terrasse could not be very old as the slope features are relatively sharp, and the reconstructed quartz input (Supplemental Fig. 1) in cores 22 and 23 does show increased values at ~1.4 ka, and between ~0.9 and ~0.7 ka, respectively. Assuming that the lake level reached the maximum level by ~1.3 ka and remained stable towards modern time, the increasing sedimentation would have decreased the water CD until modern (Fig. 8).

5.2. *Regression dynamics explained by reflectors on the radargram*

Sediment accumulation in Lake Pangodi basin seems to support the change seen in reconstructed lake levels (Figs. 8 and 9) as the total sediment accumulation during the middle Holocene, from ~8.2 to ~6.2 ka, was slightly lower in comparison to the second half of the middle Holocene (~6.2 to ~4.2 ka). This could reflect higher evaporation rates and/or warmer water temperatures and lower oxygen solubility at times of greater accumulation of organic matter. Sediment accumulation

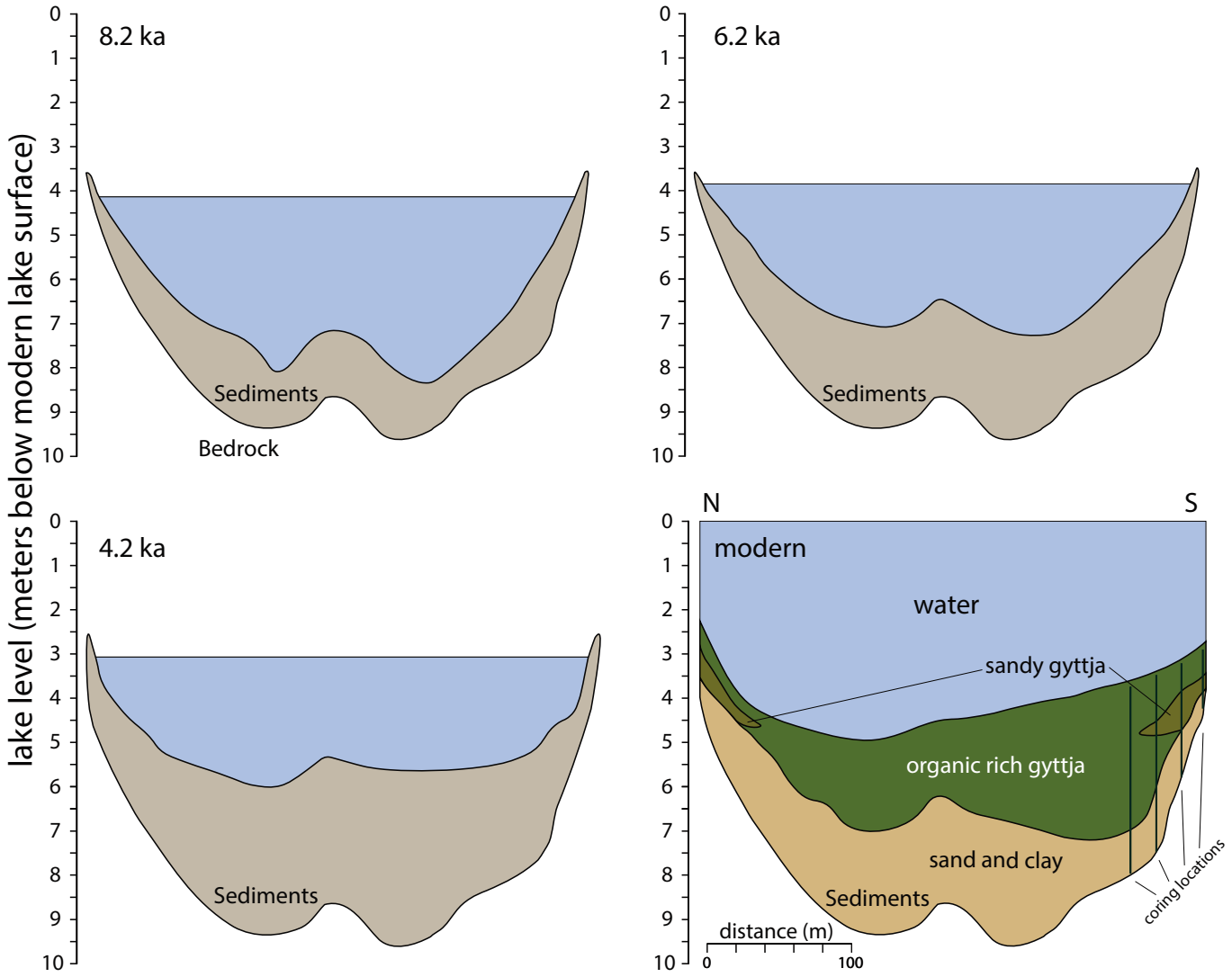

Fig. 9. Water level and water column depth changes, and sediment accumulation at Lake Pangodi during the Holocene, inferred from the modeled lake level reconstruction data (based on OM flux). The lake level represents the model mean value at the given time periods with sediment elevation extending to the maximum model uncertainty range. Top left panel shows reconstructed lake profile at ~8.2 ka, top right at ~6.2 ka and bottom left at ~4.2 ka. Modern conditions are shown on the bottom right panel where organic rich gyttja, sandy gyttja and sand/clay layers could be identified based on the four sediment cores collected from GPR transect #20 (N to S profile), shown as vertical bars on the modern panel. This figure was created based on a visual interpretation of the radargram for illustrative purposes. For average sediment-water interface depth, please refer to Fig. 8.

during the late Holocene (~4.2 to ~0.7 ka) was lower in comparison to the preceding middle Holocene. The ^{14}C-dated lake sediments plotted on our radargram (Fig. 3), the sediment composition (Figs. 5 and 6, and Table 2) and the flux model (Fig. 8) help demonstrate that, in contrast to water level elevation, the water CD at the end of the middle Holocene (~4.2 ka; 200 cm) was ~34 cm lower in comparison to the end of the early Holocene (~8.2 ka; 230 cm), ~175 cm lower than at ~0.7 ka, and similar to the 6.0 ka value (200 cm; Figs. 8 and 9).

There were climate-driven lake level variations overprinted on the sediment accumulation. The radargram (Fig. 3) shows multiple lapout features in the middle Holocene section, which can most likely be attributed to normal regression that would result in offlaps characterizing decreased lake levels (Posamentier et al., 1992). Under normal regression with constant or increasing water levels, the sediment accumulation takes place in the water environment, and the flux variation is captured in the sedimentary record. Conversely, forced regression is independent of sediment flux variations and describes decreased lake levels where the sediments would get deposited to the lake from the shore (Miall, 2010). There is truncation above 440 cm bmls (~2.5 ka) in core 22 (Fig. 3) that illustrates forced regression, adding additional confidence to our flux model that demonstrates a brief period of decreased lake levels around the same time.

5.3. *Advantages of the flux-based model*

With the Lake Pangodi water level reconstruction, we focused on the hydrological conditions in the early to middle Holocene (~8.2 ka), the middle Holocene (~6.0 ka), and the middle to late Holocene transition (~4.2 ka) with regard to modern conditions (Figs. 8 and 9). In general, the OM flux-derived lake level (elevation) model shows greater detail in comparison to using OM data only, and will therefore be used for interpretation. We find that the reconstruction shows ~310 cm and ~345 cm higher lake levels at ~8.2 ka and ~4.2 ka when comparing our OM flux-based model to the OM-based (Fig. 8), respectively. Neither one of the models suggest past lake levels reaching higher elevations than today until ~0.7 ka.

5.4. Sedimentary features on the radargram vs flux model results

The flux model is in a good agreement with the sedimentary features observed on the radargram. The lake levels discussed in this section are relative water levels below the modern lake surface. In core 24, there is an onlap before ~7.8 ka, and our model does how higher lake levels at ~8.2 ka. In core 23, offlaps above 580 cm bmls (~6.5 ka) occur at a time when our lake level model shows decreasing values (Fig. 8). Offlaps between cores 23 and 24 at 430 cm and 460 cm bmls (both likely at ~8.6 ka) support the decreased flux model values between ~8.6 and ~8.4 ka. Several reflector lines (not defined on Fig. 3) at the bottom of core 24 most likely indicate the maximum level of transgression (Miall, 2010). We also observe higher variability of lake levels in the flux model until ~7.8 ka. The offlap at 510 cm bmls (~4.3 ka) in core 22 may reflect the slightly decreased water levels that we can observe in the flux model at ~4.2 ka. Erosional truncations as evidence of decreasing lake levels can be observed at around 480 cm bmls (~2.9 ka) in core 21, above 480 cm bmls (~4.0 ka) in core 22, and between 430 cm bmls (~4.3 ka) and 400 cm bmls (~2.6 ka and above) in core 23 (Fig. 3). These lapout features support the modeled lower lake levels at ~3.3 ka (Fig. 8). Toplaps at 360 cm (~1.5 ka) in core 23 and at 410 cm bmls (~2.0 ka) basin-ward from core 22 also suggest erosional or low deposition environments afterwards. This evidence is not reflected in our flux-based lake level model (Fig. 8, see also Supplemental Fig. 1), which shows higher lake levels after 1.4 ka. Topmost sediments on the radargram show multiple continuous reflector lines that suggest consistent deposition (Fig. 3) above 320 cm bmls (~1.2 ka in core 24), which would agree with the flux model, suggesting significantly increased water levels after ~1.4 ka (Fig. 8).

5.5. Moisture balance reconstruction

The result of ~320 mm total increase in the P-E (Fig. 8 panel b) is an approximation as the lake watershed area of 7.6 km^2 is relatively large and may decrease the model output values. Likewise, more water will be pulled from the catchment into the atmosphere by transpiration as soils and larger plants establish over time, reducing inflow to the lake. There is also a large error associated with the P-E model as the average 1 standard deviation (SD) for the entire data set is ~65 mm y^{-1}. In addition, the large lake surface area to volume ratio may result in an underestimate of the P-E as the evaporation rate increases with larger surface area. The model does not account for periods of lake water overflow, introducing further error to the results. The uncertainty in the lake water residence time also affects the P-E model output. For example, increasing the water residence time from a 0.5 to 1.5-year window to a 0.5 to 5-year window would decrease the total P-E from ~320 mm to ~115 mm. Furthermore, the model assumes a constant groundwater flow to lake, introducing more uncertainty to the P-E values. Although informative, we conclude that the P-E model is merely an estimate that could be refined in the future using additional methods and proxies.

5.6. Comparison to other regional records

Based on core stratigraphy and the OM flux model results, Lake Pangodi showed an overall increasing water level elevation throughout the entire Holocene, which is partially be explained by sediment accumulation displacing water. The water level reached maximum levels at ~1.5 ka, which is supported by the topmost continuous reflector lines above 1.2 ka on our radargram (Fig. 3). Our results are similar to the reconstruction from the largest Estonian open basin lake (Lake Peipus; Fig. 1) that also suggested continuously rising water levels since ~10 ka (Hang et al., 2008). However, there was a period of decreased values in Lake Pangodi water CD between ~5.1 and ~2.4 ka (Fig. 8), and this drier period falls within the arid conditions recognized in a nearby Lake Nuudsaku between ~5.8 and ~0.7 ka (Eensalu et al., 2024). The overall trend towards higher lake levels in Estonia during the late Holocene (Fig. 8) could also be linked to the decreasing summer insolation (Harrison et al., 1993). This seasonal change in the distribution of solar insolation may have therefore resulted in increased P-E and/or in changing oceanic moisture transport. Furthermore, the differences in lake levels could have been a result of variations in the local isostatic uplift, caused by deglaciation. Comparison of different lake basins also encompasses varying lithologies of the bedrock, meaning that there are variations in hydrogeological regimes.

5.6.1. Late Pleistocene and the early Holocene

There is a possibility that Lake Pangodi water levels as well as the relative water depth during the late Pleistocene and the first half of the early Holocene (~12 ka to ~9.8 ka) could have been relatively high as suggested by the bottom-most continuous reflector lines and abundant sand in the lower part of all of the sediment cores. Lake Pangodi water CD remained >155 cm from ~9.8 ka to ~9.6 ka. Sohar and Kalm (2008) demonstrated lower lake levels in Estonia and its close vicinity (including northwest Russia, Sweden, Belarus and Karelia) persisting from the end of late Pleistocene and early Holocene until ~9.5 to ~9 ka. Our reconstruction agrees with that interpretation as the water CD at Pangodi was relatively lower (~115 cm) at around ~9.7 ka, and then rose to 190 cmby ~9.4 ka. Our result is in agreement with previously published lake level reconstructions from Poland (Pleskot et al., 2018) and southern Sweden (Digerfeldt et al., 2013). However, Punning et al. (2003) noted a lowering of lake levels in Pandivere Upland (~120 km north from Pangodi; Fig. 1) after ~9.3 ka. From ~9.6 to ~8.2 ka, Lake Pangodi reconstruction suggests rising water CD to 230 cm. Saarse et al. (1995) report the same trend of water level rise in small Estonian lakes during that time period. Terasmaa et al. (2013) demonstrate low water depths during the beginning of the Holocene in central Latvian lake Ķūži (~150 km south-west from Pangodi), after ~10.5 ka a constant rise reaching maximum values between ~9.0 and ~8.0 ka, and remaining stable thereafter until ~3.0 ka.

5.6.2. The 8.2 ka event and the middle Holocene

A ~300-year period preceding the middle Holocene (8.4 to 8.1 ka) is known as the 8.2 ka cold event that occurred due to the weakening of Northern Atlantic thermohaline circulation (Renssen et al., 2009). This was probably caused by a melt water pulse from Lake Agassiz to the North Atlantic leading to weakened zonal flow from the Atlantic and therefore increased dry conditions over northern Europe (Barber et al., 1999). Lake Pangodi middle Holocene record starts with a ~100 cm water CD decline from 230 to 130 cm between ~8.2 to ~7.7 ka (Fig. 8a and Fig. 9). Saarse et al. (1995), Sohar and Kalm (2008), Saarse and Harrison (1992) and Zernitskaya (1997) have reported similar decreases in lake levels after ~8 ka. These results may suggest that insolation-driven cold conditions were accompanied by anticyclonic conditions, and therefore decreased rainfall after ~8 ka may have caused the overall trend in decreasing lake levels. The 8.2 ka cold event has been well documented in a Lake Tõugjärv (~50 km S from Lake Pangodi; Fig. 1) record, (Veski et al., 2004) which demonstrated that the annual temperatures in Estonia decreased by ~3 °C at 8.2 ka in comparison to their researched period after the cooling (8.1 to 7.5 ka). The same study proposed greater cold and snowy winter conditions during the 8.2 ka event. An isotope-based reconstruction from Lake Äntu Sinijärv displayed significantly decreased lake water oxygen isotope ($\delta^{18}O$) values between ~8.39 and ~8.26 ka, also suggesting locally increased cold conditions (Street-Perrott et al., 2018).

The warm season insolation in Estonia during the middle Holocene was decreasing, yet remained higher than during the late Holocene. The high insolation may have caused lower P-E, and the remaining anticyclonic blocking in the northern Baltic Sea region may have reduced the amount of rainfall reaching Lake Pangodi during the middle Holocene. Our lake water CD suggests a ~110 cm increase from ~7.7 ka until ~6.6 ka. Similarly, a hydrological reconstruction from south-east Lithuania

suggests a period of drier conditions at ~7.3 ka (Stančikaitė et al., 2019). We detected a brief ~30 cm decrease in Lake Pangodi water levels from ~6.5 to ~6 ka, also recognized as a warm and dry period in southern Sweden and Denmark at ~6.5 ka (Seppä et al., 2005; Brown et al., 2012). The water CD increase after ~7.7 ka could be connected to an intensified AMOC (Zhang et al., 2016), which would have led to increased moisture transport (similar to the positive phase of modern-day NAO), and therefore enough precipitation to elevate Lake Pangodi water CD by over a meter by ~6.8 ka at Pangodi.

During the second half of the middle Holocene (6.2 to 4.2 ka) Lake Pangodi water CD remained above 175 cm. After ~6.2 ka, the lake water CD increased from 200 cm to 250 cm bmls by 5.7 ka, similar to the water level rise seen in the Lithuanian bog record (Stančikaitė et al., 2019). Lake Pangodi water remained at a relatively higher level until ~5 ka, yet the water column depth was slightly decreasing due to accumulating sediments. Our data are supported by Punning et al. (2005) who report increased water level in Lake Juusa (~20 km south from Pangodi; Fig. 1) at that time, which they interpreted as water level high-stand as a result of increased precipitation and decreased summer insolation (Fig. 8). Lake Pangodi water CD then decreased from 200 cm at ~5.0 ka to 175 cm at ~4.9 ka, indicating drier conditions. The Lithuanian bog record also reports driest conditions between 5.1 and 4.9 ka (Stančikaitė et al., 2019). However, Terasmaa et al. (2013) suggest the lake levels in Lake Ķūži (Latvia) during that time were rather high and relatively stable. Seppä and Poska (2004) suggest there was a cooling trend in Estonia starting ~5.3 ka, also associated with decreasing lake levels (Sohar and Kalm, 2008), and possibly decreased westerly air flow. Lake Pangodi water CD then slightly rose to ~200 cm by ~4.2 ka. The onset of wet conditions in Estonia therefore likely preceded the 4.2 ka event by several hundred years. This rise in water levels contrasts southern Swedish hydroclimate reconstruction which suggested predominantly dry conditions between 4.8 ka and 4.4 ka (De Jong et al., 2009).

In general, the increasing water level trend at Lake Pangodi is in an agreement with a nearby open-basin Lake Nuudsaku isotope record which suggests the middle Holocene may have experienced a trend of increasing warm season precipitation (Stansell et al., 2017) and higher relative humidity (Eensalu et al., 2024). The summer precipitation could have therefore likely been higher as our record generally shows increasing water levels throughout the middle Holocene, although as discussed above, Lake Pangodi is relatively sensitive to evaporation. Further, a climate modeling study (Mauri et al., 2014) argued that the middle Holocene moisture availability in Europe was mostly influenced by increased cold season precipitation, which would be well characterized by a positive phase of the NAO. Our results could support that finding because despite the water level increasing relative to the modern lake surface, Lake Pangodi water CD during the ~8.0 to ~5.8 ka period was greater than during the latter half of the middle Holocene (Fig. 9). However, it has been suggested that not all precipitation droughts are apparent in lake water changes (Brunner and Chartier-Rescan, 2024). Nonetheless, the contrasting results during the middle Holocene in this region demonstrate that hydroclimate variability likely experienced high spatial variability.

5.6.3. *The late Holocene*

The late Holocene in the northern Hemisphere became colder due to decreased warm season insolation (Routson et al., 2019). Previous research has also suggested that the increased cyclonic activity and westerly winds may have altered the hydrological conditions in Europe (Seppä and Birks, 2001). The lowest late Holocene water CD values of 170 cm at Lake Pangodi were detected at ~3.3 ka (Fig. 8 panel b). Punning et al. (2005) report decreased Lake Juusa water levels at ~3.2 ka, Saarse et al. (1995) in twelve small Estonian lakes from ~4.5 to ~3.8 ka (Sohar and Kalm, 2008), and Saarse and Rajamae (1997) 2.5 to 3 m lower lake levels in Haanja highlands (~70 km SSE from Pangodi; Fig. 1) at ~3.7 ka. Seppä and Poska (2004) derive from Lake Raigastvere (50 km north from Pangodi; Fig. 1) pollen analyses that there was a potential cold event at ~3.2 ka, and Street-Perrott et al. (2018) discuss a similar unnamed cold event peaking at ~3.3 ka, inferred from stable oxygen isotope proxy from lake Äntu Sinijärv. The $\delta^{18}O$ proxy of Lake Igelsjön in Sweden at ~3.4 ka also shows decreased values of >3 ‰ in comparison to 4.0 ka, which may be connected to the same cold conditions (Hammarlund et al., 2003). Based on our model, we suggest that this multi-centennial cold period at Lake Pangodi was relatively drier. This event also coincides with a 1 °C temperature decrease noted in the pollen records from the Baltic Sea basin between 4.3 and 3.3 ka (Borzenkova et al., 2015).

A steady increase in the Lake Pangodi record from ~3.3 to ~2.5 ka suggests water CD increasing to ~250 cm. Likewise, Luik and Tõnisson (2023) find that the period between ~3.3 to ~3.0 ka in Estonia experienced increased storminess. This may be related to increasing cold season insolation in the northern Hemisphere resulting in higher winter P-E. It has also been noted that the AMOC strength was briefly reduced at ~3 ka (Telesiński et al., 2015), which may have led to decreased air mass transport to northern Europe. Similar trends of rising lake levels after ~2.5 ka has also been observed in various small Estonian lakes during the same time period (Saarse et al., 1995; Sohar and Kalm, 2008). Contrastingly, Terasmaa et al. (2013) demonstrate a 3 m decline in lakes water depth in central Latvian lake starting from ~3.0 ka BP. The brief period in the Lake Pangodi reconstruction between ~2.5 and ~2.4 ka suggests decreased water CD, and decreased P-E (Fig. 8).

The ~130 cm water CD increase at Lake Pangodi from ~2.4 ka (160 cm) to ~2.2 ka (290 cm) suggests increased P-E and a possible shift towards wetter conditions. This trend was particularly pronounced in Viitna lakes (~150 km north from Pangodi; Fig. 1) at ~2.6 to ~1.9 ka which has been attributed to increased cool and wet conditions (Punning et al., 1987). Saarse et al. (1998) also report that lakes in Haanja highlands experienced increased precipitation after ~2.2 ka and reduced evapotranspiration rates, based on pollen analyses. Interestingly, Luik and Tõnisson (2023) report stable and dry conditions in Estonia between ~2.4 and ~2.2 ka.

The decreasing water column depth between ~2.2 and ~1.5 ka (from 290 to 230 cm) could imply a several centennial decrease in cyclonic/wet conditions, resulting in slightly increased evaporation in the basin, or a decrease in precipitation. Higher Lake Pangodi water CD after ~1.4 ka indicate increased P-E. Saarse and Rajamae (1997) suggested higher lake levels starting already at ~1.7 ka, however, the modeled Lake Pangodi water level displays large error ranges after ~1.4 ka (Figs. 4, 8). Our OM flux data suggested that sub-littoral to deep-water conditions persisted throughout the record until the modern time with some sub-littoral sediments identified in core 22 at ~1 ka. In addition to the sedimentary evidence discussed above suggesting lower lake levels at around ~0.9 ka, this indicates slightly drier conditions prevailing at Lake Pangodi during the Medieval Climate Anomaly (MCA; ~1 to ~0.7 ka).

6. Conclusions

Comparison of the Lake Pangodi sediment facies and the lake level model reveal variable lake levels since ~9.8 ka. Lake Pangodi water column depth during the early and middle Holocene were more than 2.0 m below modern values. We identify several centennial-scale fluctuations, similar to what have been identified from sedimentary archives in northern Europe during Holocene. Sandy layers in the Lake Pangodi record document the most notable reduction in lake levels between ~8.2 and ~7.7 ka when the lake level decreased by ~1.0 m, likely due to reduced precipitation caused by westerly air flow and cold conditions. Our middle Holocene reconstruction of Lake Pangodi water level exhibits similar hydrological changes to several archives in close proximity to the study area in the Baltic region, suggesting that the regional hydroclimate was affected by the same drivers. Conversely, some of the contrasting results from Scandinavia indicate that these areas were affected by different hydroclimate driving mechanisms. In comparison to the rest of the record, our lake level model suggests the most abrupt

rise in water levels at ~1.4 ka. Our findings underscore the complex interplay of regional hydroclimate drivers, shedding light on the nuanced spatiotemporal variability in the high-latitude region and emphasizing the importance of unravelling the mechanisms underlying these geographic differences.

CRediT authorship contribution statement

Mariliis Eensalu: Writing – review & editing, Writing – original draft, Visualization, Validation, Supervision, Resources, Project administration, Methodology, Investigation, Funding acquisition, Formal analysis, Data curation, Conceptualization. **Nathan D. Stansell:** Writing – review & editing, Writing – original draft, Supervision, Resources, Project administration, Methodology, Investigation, Funding acquisition, Conceptualization. **Hannes Tõnisson:** Writing – review & editing, Supervision, Methodology, Investigation, Conceptualization. **Jaanus Terasmaa:** Writing – review & editing, Methodology, Investigation, Conceptualization. **Egert Vandel:** Writing – review & editing, Methodology, Investigation, Conceptualization. **Tiit Vaasma:** Writing – review & editing, Methodology, Investigation, Conceptualization. **Eric S. Klein:** Writing – review & editing, Methodology, Investigation, Conceptualization. **Cameron R. Kuhle:** Writing – review & editing, Methodology, Investigation, Conceptualization. **Daniel B. Nelson:** Writing – review & editing, Methodology, Investigation, Conceptualization.

Declaration of competing interest

Nathan D. Stansell reports financial support was provided by National Science Foundation. Hannes Tonisson reports financial support was provided by Estonian Research Council. Mariliis Eensalu reports financial support was provided by Geological Society of America. Mariliis Eensalu reports financial support was provided by American Philosophical Society. If there are other authors, they declare that they have no known competing financial interests or personal relationships that could have appeared to influence the work reported in this paper.

Data availability

Data will be made available on request.

Acknowledgements

This research was funded by the U.S. National Science Foundation, International Research Experiences for Students (IRES) grant (OISE-1827135), and Estonian Research Council grant PRG1471. We thank the IRES participants for help during the field work. Funding was also provided by the Goldich grant by Northern Illinois University, graduate student research grants by the Geological Society of America (GSA), and Lewis and Clark Field Scholarship by the American Philosophical Society, awarded to ME.

Appendix A. Supplementary data

Supplementary data to this article can be found online at https://doi.org/10.1016/j.palaeo.2024.112531.

References

Abbott, M.B., Stafford, T.W., 1996. Radiocarbon geochemistry of modern and Ancient Arctic lake systems, Baffin Island, Canada. Quat. Res. 45, 300–311.
Barber, D.C., Jennings, A.E., Andrews, J.T., Kerwin, M.W., Morehead, M.D., Dyke, A.S., Hillaire-Marcel, C., 1999. Forcing of the cold event of 8,200 years ago by catastrophic drainage of Laurentide lakes. Nature 400, 13–15.
Björck, S., Kromer, B., Johnsen, S., Bennike, O., Hammarlund, D., Lemdahl, G., Possnert, G., Rasmussen, T.L., Wohlfarth, B., Hammer, C.U., Spurk, M., 1996. Synchronized terrestrial-atmospheric deglacial records around the North Atlantic. Science 274, 1155–1160.
Blaauw, M., Christen, J.A.. rbacon: Age-Depth Modelling Using Bayesian Statistics. R Package Version 2.3.4. https://CRAN.R-project.org/package=rbacon.
Boggs Jr., S., 2015. Principles of Stratigraphy and Sedimentology. John Wiley & Sons.
Borzenkova, I., Zorita, E., Borisova, O., Kalniņa, L., Kisielienė, D., Koff, T., Kuznetsov, D., Lemdahl, G., Sapelko, T., Stančikaitė, M., Subetto, D., 2015. Climate change during the Holocene (past 12,000 years). In: Second Assessment of Climate Change for the Baltic Sea Basin, pp. 25–49.
Brown, K.J., Seppä, H., Schoups, G., Fausto, R.S., Rasmussen, P., Birks, H.J.B., 2012. A spatio-temporal reconstruction of holocene temperature change in southern Scandinavia. Holocene 22, 165–177.
Brunner, M.I., Chartier-Rescan, C., 2024. Drought spatial extent and dependence increase during drought propagation from the atmosphere to the hydrosphere. Geophys. Res. Lett. 51.
Christie-Blick, N., 1991. Onlap, offlap, and the origin of unconformity-bounded depositional sequences. Mar. Geol. 97, 35–56.
Corradini, E., Wilken, D., Zanon, M., Groß, D., Lübke, H., Panning, D., Dörfler, W., Rusch, K., Mecking, R., Erkul, E., Pickartz, N., Feeser, I., Rabbel, W., 2020. Reconstructing the palaeoenvironment at the early Mesolithic site of Lake Duvensee: ground-penetrating radar and geoarchaeology for 3D facies mapping. Holocene 30, 820–833.
De Jong, R., Hammarlund, D., Nesje, A., 2009. Late Holocene effective precipitation variations in the maritime regions of south-West Scandinavia. Quat. Sci. Rev. 28.
Dean Jr., W., 1974. Determination of carbonate and organic matter in calcareous sediments and sedimentary rocks by loss on ignition: comparison with other methods. SEPM J. Sediment. Res. 44.
Digerfeldt, G., 1988. Reconstruction and regional correlation of Holocene lake-level fluctuations in Lake Bysjön, South Sweden. Boreas 17, 165–182.
Digerfeldt, G., Björck, S., Hammarlund, D., Persson, T., 2013. Reconstruction of Holocene Lake-Level Changes in Lake Igelsjön, Southern Sweden, (*GFF* 135).
EEA, 2024. Climate Normals. Est Environ Agency Clim Norm.
Eensalu, M., Nelson, D.B., Buczynska, A., Rach, O., Luoto, T.P., Poska, A., Klein, E.S., Stansell, N.D., 2024. Holocene hydroclimate variability of the Baltic region inferred from stable isotopes, d-excess and multi-proxy data at lake Nuudsaku, Estonia (NE Europe). Quat. Sci. Rev. 334.
Gat, J.R., 1996. Oxygen and hydrogen isotopes in the hydrologic cycle. Annu. Rev. Earth Planet. Sci. 24, 225–262.
Hammarlund, D., Björck, S., Buchardt, B., Israelson, C., Thomsen, C.T., 2003. Rapid hydrological changes during the Holocene revealed by stable isotope records of lacustrine carbonates from Lake Igelsjön, southern Sweden. Quat. Sci. Rev. 22, 353–370.
Hang, T., Kalm, V., Kihno, K., Milkevičius, M., 2008. Pollen, diatom and plant macrofossil assemblages indicate a low water level phase of Lake Peipsi at the beginning of the Holocene. Hydrobiologia 599, 13–21.
Harrison, S.P., Prentice, I.C., Guiot, J., 1993. Climatic controls on Holocene lake-level changes in Europe. Clim. Dyn. 8.
Heikkilä, M., Seppä, H., 2010. Holocene climate dynamics in Latvia, eastern Baltic region: a pollen-based summer temperature reconstruction and regional comparison. Boreas 39, 705–719.
Huber, E., Hans, G., 2018. RGPR - an open-source package to process and visualize GPR data. In: 2018 17th International Conference on Ground Penetrating Radar, GPR 2018.
Jaagus, J., 2003. Climate change tendencies in Estonia in relation with changes in atmospheric circulation during the second half of the 20th century. In: Jaagus, J. (Ed.), Studies on Climate of Estonia. University of Tartu, Institute of Geography, pp. 78–100.
Jaagus, J., 2006. Climatic changes in Estonia during the second half of the 20th century in relationship with changes in large-scale atmospheric circulation. Theor. Appl. Climatol. 83, 77–88.
Jaagus, J., Kull, A., 2011. Changes in surface wind directions in Estonia during 1966-2008 and their relationships with large-scale atmospheric circulation. Est. J. Earth Sci. 60, 220–231.
Jaagus, J., Sepp, M., Tamm, T., Järvet, A., Mõisja, K., 2017. Trends and regime shifts in climatic conditions and river runoff in Estonia during 1951-2015. Earth Syst. Dynam. 8, 963–976.
Kalm, V., Raukas, A., Rattas, M., Lasberg, K., 2011. Pleistocene glaciations in Estonia. In: Developments in Quaternary Science, pp. 95–104.
Keskkonnaagentuur, 2022. Estonian Nature Information System (EELIS).
King, C.A.M., Williams, W.W., 1949. The formation and movement of sand bars by wave action. Geogr. J. 113, 70.
Kipfer, B.A., 2021. Munsell soil color chart. In: Encyclopedic Dictionary of Archaeology, p. 903.
Klein, E., Berg, E.E., Dial, R., 2005. Wetland drying and succession across the Kenai Peninsula Lowlands, south-Central Alaska. Can. J. For. Res. 35, 1931–1941.
Kylander, M.E., Ampel, L., Wohlfarth, B., Veres, D., 2011. High-resolution X-ray fluorescence core scanning analysis of Les Echets (France) sedimentary sequence: new insights from chemical proxies. J. Quat. Sci. 26, 109–117.
Lamb, P.J., Peppler, R.A., 1987. North Atlantic oscillation: concept and an application. Bull. Am. Meteorol. Soc. 68, 1218–1225.
Lê, S., Josse, J., Husson, F., 2008. FactoMineR: an R package for multivariate analysis. J. Stat. Softw. 25.
Li, M., Hinnov, L., Kump, L., 2019. Acycle: time-series analysis software for paleoclimate research and education. Comput. Geosci. 127, 12–22.
Loeppert, R.H., Suarez, D.L., 1996. Carbonate and gypsum. In: Methods of Soil Analysis: Part 3 Chemical Methods, 5, pp. 437–474.
Luik, K., Tõnisson, H., 2023. Climatic Differences Between Estonia and Svalbard During the Second Half of the Holocene.

Magny, M., Bégeot, C., Guiot, J., Peyron, O., 2003. Contrasting patterns of hydrological changes in europe in response to holocene climate cooling phases. Quat. Sci. Rev. 22, 1589–1596.
Marshall, J., Kushnir, Y., Battisti, D., Chang, P., Czaja, A., Dickson, R., Hurrell, J., McCartney, M., Saravanan, R., Visbeck, M., 2001. North Atlantic climate variability: phenomena, impacts and mechanisms. Int. J. Climatol. 21, 1863–1898.
Marsicek, J.P., Shuman, B., Brewer, S., Foster, D.R., Oswald, W.W., 2013. Moisture and temperature changes associated with the mid-Holocene Tsuga decline in the northeastern United States. Quat. Sci. Rev. 80, 129–142.
Mason, I.M., Guzkowska, M.A.J., Rapley, C.G., Street-Perrott, F.A., 1994. The response of lake levels and areas to climatic change. Clim. Chang. 27, 161–197.
Mauri, A., Davis, B.A.S., Collins, P.M., Kaplan, J.O., 2014. The influence of atmospheric circulation on the mid-Holocene climate of Europe: a data-model comparison. Clim. Past 10, 1925–1938.
Miall, A.D., 2010. The Geology of Stratigraphic Sequences: Second Edition.
Mitchum, R.M., 1977. Seismic stratigraphy and global changes of sea level, part 11 glossary of terms used in seismic stratigraphy. In: Seismic Stratigraphy — Applications to Hydrocarbon Exploration.
Morley, A., Rosenthal, Y., DeMenocal, P., 2014. Ocean-atmosphere climate shift during the mid-to-late Holocene transition. Earth Planet. Sci. Lett. 388, 18–26.
Nestor, H., Einasto, R., Raukas, A., Teedumäe, A., 1997. Geology and Mineral Resources of Estonia, pp. 89–106.
Newby, P.E., Shuman, B.N., Donnelly, J.P., MacDonald, D., 2011. Repeated century-scale droughts over the past 13,000 yr near the Hudson River watershed, USA. Quat. Res. 75, 523–530.
Parish, M.C., Wolf, K.D., Higuera, P.E., Shuman, B.N., 2022. Holocene water levels of Silver Lake, Montana, and the hydroclimate history of the Inland Northwest. Quat. Res. 110, 54–66.
Parry, L.E., West, L.J., Holden, J., Chapman, P.J., 2014. Evaluating approaches for estimating peat depth. J. Geophys. Res. Biogeosci. 119, 567–576.
Paul, A., Schulz, M., 2002. Holocene climate variability on centennial-to-millennial time scales: 2. Internal and forced oscillations as possible causes. In: Climate Development and History of the North Atlantic Realm. Springer, Berlin Heidelberg, pp. 55–73.
Pleskot, K., Tjallingii, R., Makohonienko, M., Nowaczyk, N., Szczuciński, W., 2018. Holocene paleohydrological reconstruction of Lake Strzeszyńskie (western Poland) and its implications for the central European climatic transition zone. J. Paleolimnol. 59, 443–459.
Posamentier, H.W., Allen, G.P., James, D.P., Tesson, M., 1992. Forced regressions in a sequence stratigraphic framework: concepts, examples, and exploration significance. Am. Assoc. Pet. Geol. Bull. 76, 1687–1709.
Poska, A., Saarse, L., Koppel, K., Nielsen, A.B., Avel, E., Vassiljev, J., Väli, V., 2014. The Verijärv area, South Estonia over the last millennium: a high resolution quantitative land-cover reconstruction based on pollen and historical data. Rev. Palaeobot. Palynol. 207, 5–17.
Pribyl, P., Shuman, B.N., 2014. A computational approach to quaternary lake-level reconstruction applied in the central Rocky Mountains, Wyoming, USA. Quat. Res. 82, 249–259.
Punning, J.M., Ilomets, M., Koff, T., Paap, Ü., Rajamäe, R., 1987. On the development of Lake Ümarjarv (NE Estonia) in the Holocene. Palaeoecol. Temp. Zo II, 123–136.
Punning, J.M., Kangur, M., Koff, T., Possnert, G., 2003. Holocene lake-level changes and their reflection in the paleolimnological records of two lakes in northern Estonia. J. Paleolimnol. 29, 167–178.
Punning, J.M., Koff, T., Kadastik, E., Mikomägi, A., 2005. Holocene Lake level fluctuations recorded in the sediment composition of Lake Juusa, southeastern Estonia. J. Paleolimnol. 34, 377–390.
Räisänen, J., 2016. Future climate change in the Baltic Sea Region and environmental impacts. Oxford Res. Encycl. Clim. Sci. 1, 1–39.
Raukas, A., 2009. When and how did the continental ice retreat from Estonia? Quat. Int. 207, 50–57.
Reimer, P.J., Austin, W.E.N., Bard, E., Bayliss, A., Blackwell, P.G., Bronk, Ramsey C., Butzin, M., Cheng, H., Edwards, R.L., Friedrich, M., Grootes, P.M., Guilderson, T.P., Hajdas, I., Heaton, T.J., Hogg, A.G., Hughen, K.A., Kromer, B., Manning, S.W., Muscheler, R., Palmer, J.G., Pearson, C., Van Der Plicht, J., Reimer, R.W., Richards, D.A., Scott, E.M., Southon, J.R., Turney, C.S.M., Wacker, L., Adolphi, F., Büntgen, U., Capano, M., Fahrni, S.M., Fogtmann-Schulz, A., Friedrich, R., Köhler, P., Kudsk, S., Miyake, F., Olsen, J., Reinig, F., Sakamoto, M., Sookdeo, A., Talamo, S., 2020. The IntCal20 Northern hemisphere radiocarbon age calibration curve (0-55 cal kBP). Radiocarbon 62, 725–757.
Renssen, H., Seppä, H., Heiri, O., Roche, D.M., Goosse, H., Fichefet, T., 2009. The spatial and temporal complexity of the holocene thermal maximum. Nat. Geosci. 2.
Renssen, H., Seppä, H., Crosta, X., Goosse, H., Roche, D.M., 2012. Global characterization of the Holocene thermal maximum. Quat. Sci. Rev. 48, 7–19.
Rodionov, S.N., 2004. A sequential algorithm for testing climate regime shifts. Geophys. Res. Lett. 31, 2–5.
Rossby, T., 1999. On gyre interactions. Deep Res. Part II Top. Stud. Oceanogr. 46, 139–164.
Routson, C.C., McKay, N.P., Kaufman, D.S., Erb, M.P., Goosse, H., Shuman, B.N., Rodysill, J.R., Ault, T., 2019. Mid-latitude net precipitation decreased with Arctic warming during the Holocene. Nature 568, 83–87.
Saarse, L., Harrison, S.P., 1992. Holocene lake-level changes in the eastern Baltic region. Est. Man. Nat. 6.
Saarse, L., Rajamae, R., 1997. Holocene vegetation and climatic change on the Haanja Heights, SE Estonia. Proc. Est. Acad. Sci. Geol. 46, 75–92.
Saarse, L., Heinsalu, A., Veski, S., 1995. Palaeoclimatic interpretation of the Holocene litho-and biostratigraphic proxy data from Estonia. In: Conf PAST, Present Futur Clim, p. 102.
Saarse, L., Poska, A., Kaup, E., Heinsalu, A., 1998. Holocene environmental events in the Viitna area, North Estonia. Proc. Est. Acad. Sci. Geol. 47, 31–44.
Seppä, H., Birks, H.J.B., 2001. July mean temperature and annual precipitation trends during the Holocene in the fennoscandian tree-line area: pollen-based climate reconstructions. Holocene 11, 527–539.
Seppä, H., Poska, A., 2004. Holocene annual mean temperature changes in Estonia and their relationship to solar insolation and atmospheric circulation patterns. Quat. Res. 61, 22–31.
Seppä, H., Hammarlund, D., Antonsson, K., 2005. Low-frequency and high-frequency changes in temperature and effective humidity during the Holocene in south-Central Sweden: Implications for atmospheric and oceanic forcings of climate. Clim. Dyn. 25, 285–297.
Seppä, H., Bjune, A.E., Telford, R.J., Birks, H.J.B., Veski, S., 2009. Last nine-thousand years of temperature variability in Northern Europe. Clim. Past 5, 523–535.
Shirley, I.A., Mekonnen, Z.A., Grant, R.F., Dafflon, B., Hubbard, S.S., Riley, W.J., 2022. Rapidly changing high-latitude seasonality: implications for the 21st century carbon cycle in Alaska. Environ. Res. Lett. 17.
Sohar, K., Kalm, V., 2008. A 12.8-ka-long palaeoenvironmental record revealed by subfossil ostracod data from lacustrine freshwater tufa in Lake Sinijärv, northern Estonia. J. Paleolimnol. 40, 809–821.
Spencer, R.J., Baedecker, M.J., Eugster, H.P., Forester, R.M., Goldhaber, M.B., Jones, B. F., Kelts, K., Mckenzie, J., Madsen, D.B., Rettig, S.L., Rubin, M., Bowser, C.J., 1984. Great Salt Lake, and precursors, Utah: the last 30,000 years. Contrib. Mineral. Petrol. 86, 321–334.
Stančikaitė, M., Gedminienė, L., Edvardsson, J., Stoffel, M., Corona, C., Gryguc, G., Uogintas, D., Zinkutė, R., Skuratovič, Ž., Taraškevičius, R., 2019. Holocene vegetation and hydroclimatic dynamics in SE Lithuania – Implications from a multi-proxy study of the Čepkeliai bog. Quat. Int. 501, 219–239.
Stansell, N.D., Klein, E.S., Finkenbinder, M.S., Fortney, C.S., Dodd, J.P., Terasmaa, J., Nelson, D.B., 2017. A stable isotope record of Holocene precipitation dynamics in the Baltic region from Lake Nuudsaku, Estonia. Quat. Sci. Rev. 175, 73–84.
Street-Perrott, F.A., Holmes, J.A., Robertson, I., Ficken, K.J., Koff, T., Loader, N.J., Marshall, J.D., Martma, T., 2018. The Holocene isotopic record of aquatic cellulose from Lake Äntu Sinijärv, Estonia: influence of changing climate and organic-matter sources. Quat. Sci. Rev. 193, 68–83.
Telesiński, M.M., Bauch, H.A., Spielhagen, R.F., Kandiano, E.S., 2015. Evolution of the central Nordic Seas over the last 20 thousand years. Quat. Sci. Rev. 121, 98–109.
Terasmaa, J., 2011. Lake basin development in the Holocene and its impact on the sedimentation dynamics in a small lake (southern Estonia). Est. J. Earth Sci. 60, 159–171.
Terasmaa, J., Puusepp, L., Marzecová, A., Vandel, E., Vaasma, T., Koff, T., 2013. Natural and human-induced environmental changes in Eastern Europe during the Holocene: a multi-proxy palaeolimnological study of a small Latvian lake in a humid temperate zone. J. Paleolimnol. 49, 663–678.
Vaasma, T., Vandel, E., 2024. Eesti Väikejärvede Batümeetriline Seire 2022, Tallinn.
Veski, S., Seppä, H., Ojala, A.E.K., 2004. Cold event at 8200 yr B.P. Recorded in annually laminated lake sediments in eastern Europe. Geology 32, 681–684.
Walker, M.J.C., Berkelhammer, M., Björck, S., Cwynar, L.C., Fisher, D.A., Long, A.J., Lowe, J.J., Newnham, R.M., Rasmussen, S.O., Weiss, H., 2012. Formal subdivision of the Holocene Series/Epoch: a discussion paper by a working group of INTIMATE (integration of ice-core, marine and terrestrial records) and the subcommission on quaternary stratigraphy (international commission on stratigraphy). J. Quat. Sci. 27, 649–659.
Wibig, J., 1999. Precipitation in Europe in relation to circulation patterns at the 500 hPa level. Int. J. Climatol. 19, 253–269.
Zernitskaya, V.P., 1997. The evolution of lakes in the poles'ye in the late glacial and Holocene. Quat. Int. 41–42, 153–160.
Zhang, Y., Renssen, H., Seppä, H., 2016. Effects of melting ice sheets and orbital forcing on the early Holocene warming in the extratropical Northern Hemisphere. Clim. Past 12, 1119–1135.